Adaptive Power Control for Dense RFID Networks

Bernard Amoah, Xiangyu Wang, Jian Zhang, Shiwen Mao, Senthilkumar C.G. Periaswamy, Justin Patton

***Abstract*—Adaptive power control is a critical challenge in dense radio frequency identification (RFID) environments, where uncontrolled power levels can lead to excessive interference, energy inefficiency, and reduced system performance. This paper presents a robust and scalable adaptive power control framework that dynamically adjusts transmit power levels to optimize energy efficiency, minimize interference, and enhance system throughput. The proposed framework leverages an optimization-driven approach based on real-time environmental feedback, ensuring compliance with regulatory constraints while maintaining optimal performance. A multi-objective optimization strategy is employed to balance several key metrics, including throughput, energy consumption, and fairness, with a Pareto front analysis demonstrating superior trade-offs compared to fixed power strategies. The effectiveness of the proposed approach is validated through extensive simulations and real-world experiments using universal software radio peripheral (USRP) devices in dense RFID deployments. The results show that our framework achieves a 34% reduction in cumulative interference, a 15% improvement in energy efficiency, and a 20% increase in throughput compared to baseline fixed power methods. Furthermore, it converges rapidly, even in dynamic and high-density networks. These improvements make it highly scalable and adaptable to varying reader densities, ensuring reliable performance in large-scale RFID applications such as supply chain management and industrial automation.**

***Keywords*—adaptive power control, radio frequency identification (RFID), interference management, energy efficiency, multi-objective optimization, scalability**

Manuscript received Jun. 04, 2025; revised Jun. 20, 2025; accepted Jun. 20, 2025. This work is supported in part by the United States National Science Foundation under Grants CCSS-2245607 and CCSS-2245608, and by the Wireless Engineering Research and Education Center and RFID Lab at Auburn University. The associate editor coordinating the review of this paper and approving it for publication was W. Zhang.

B. Amoah, S. W. Mao. Department of Electrical and Computer Engineering, Auburn University, Auburn, AL 36849-5201, USA (e-mail: bza0066@auburn.edu; smao@ieee.org).

J. Zhang. Department of Electrical and Computer Engineering, Kennesaw State University, Kennesaw, GA 30144, USA (e-mail: jianzhang@ieee.org).

X. Y. Wang, S. C. G. Periaswamy, J. Patton. RFID Lab, Auburn University, Auburn, AL 36849, USA (e-mail: xzw0042@auburn.edu; szc0089@auburn.edu; jbp0033@auburn.edu).

I. Introduction

Radio frequency identification (RFID) technology is a ubiquitous tool for enabling automatic identification and tracking of objects across a wide range of applications, including logistics, retail, healthcare, and industrial automation[1-4]. Its ability to provide real-time visibility and data collection has revolutionized operations in these industries. However, as RFID systems scale to meet the demands of dense deployment environments—such as large warehouses, retail stores, and manufacturing facilities—new challenges emerge, particularly in interference management, power efficiency, and system reliability[5].

Dense RFID environments are characterized by the coexistence of multiple RFID readers and a high density of tags operating within overlapping interrogation zones. While this deployment scenario offers the potential for enhanced operational efficiency, it also introduces significant technical challenges. RFID readers operating on the same or overlapping frequencies interfere with each other, degrading communication performance and leading to missed tag reads[6]. Simultaneous interrogation by multiple readers can overwhelm tags, reducing the accuracy and efficiency of the system. Fixed power systems often transmit at levels that are either excessive or insufficient for the dynamic conditions of dense environments, wasting energy and increasing interference[7-8].

In traditional RFID systems, readers operate at fixed transmission power levels, which are determined during system installation and rarely adapt to changing environmental conditions. While fixed power allocation simplifies system design, it introduces several limitations. In environments with low tag density or short reader-to-tag distances, fixed high power levels lead to unnecessary energy consumption and increased reader-to-reader interference (RRI). Conversely, in environments with high tag density or large distances, fixed low power levels may result in reduced tag detection and incomplete data collection. Fixed systems are inadequate for responding to real-time variations in environmental factors such as tag mobility, interference from nearby devices, or varying network congestion[5,9-10].

To address the limitations of fixed power systems, there is a need for intelligent power control mechanisms that dynami-

cally adjust reader transmission power in response to environmental conditions[11]. Adaptive power control offers a promising solution by dynamically tuning power levels to reduce reader-to-reader interference and reader-to-tag collisions, adjusting power to the minimum required for reliable communication, thereby conserving energy and enabling the efficient operation of a large number of readers and tags in dense environments.

While several adaptive power control strategies have been proposed, many existing solutions have limitations. Some approaches do not adequately consider real-time variations in environmental conditions, leading to delayed responses or suboptimal power adjustments[12-13]. Others may not efficiently integrate interference management and network congestion control, resulting in partial solutions that fail to maximize overall system performance[5,14].

This paper introduces a novel adaptive power control framework (an advanced version of our RFIDNet RCC subprotocol presented in Ref. [15]), designed to improve the robustness and efficiency of RFID systems in dense deployment scenarios. The proposed approach leverages real-time feedback from environmental conditions, such as tag distance, network congestion, and interference levels, to optimize power allocation dynamically. Key features of the framework include continuous measurement of signal strength, interference, and tag response rates to inform power adjustments and a mathematically grounded approach to minimize interference and maximize tag detection reliability and support for dense environments with multiple readers and tags, ensuring consistent performance under varying conditions. Our approach is built upon fundamental principles such as carrier sense multiple access (CSMA) to ensure that communication resources are allocated efficiently across readers and tags[2]. The proposed framework addresses critical challenges in RFID systems, paving the way for improved performance in applications such as enhancing inventory tracking and reducing missed tag reads in dense warehouses, ensuring reliable monitoring of medical equipment, and patient tracking in hospitals, and supporting the robust operation of RFID-based systems in complex manufacturing environments. Unlike existing solutions, this paper presents a framework that explicitly accounts for dynamic tag mobility, overlapping reader coverage, and real-time environmental feedback, offering a comprehensive solution to the challenges of dense RFID deployments. The key contributions made in this paper are as follows.

- A Fully Adaptive Framework with Real-Time Feedback: Unlike static or threshold-based methods, we propose a real-time feedback loop that leverages tag response statistics, interference measurements, and signal quality to adapt transmission power dynamically.
- Game-Theoretic Optimization Strategy: We formulate power allocation as a non-cooperative game and prove convergence to a stable Nash equilibrium using Lyapunov and contraction mapping techniques, ensuring theoretical soundness and practical convergence.
- Dynamic State Transition Mechanism: Readers operate in adaptive modes (active, idle, power-adjustment), enabling the framework to balance performance and energy use, even under reader failures and changing tag densities.
- Comprehensive Validation in Real Hardware and Simulation: The framework is validated on a dense universal software radio peripheral (USRP)-based RFID testbed and large-scale MATLAB simulations, achieving superior performance in throughput, latency, energy efficiency, and fairness.

These contributions collectively provide a scalable and field-deployable solution for dense RFID networks.

The remainder of this paper is structured as follows. Section II reviews the existing interference management, power control, and collision mitigation techniques. Section III formalizes the problem and introduces the key metrics driving the design of the proposed adaptive power control framework. Section IV details the proposed framework. Section V presents the performance evaluation of the proposed framework through real-world experimentation with USRP, while section VI presents the performance evaluation of the proposed framework through simulations. Section VII discusses the results and their implications. Section VIII concludes the paper. Appendix A provides a mathematical analysis of the algorithm's stability and convergence, demonstrating its efficiency and robustness. Appendix B examines the scalability of the proposed framework in varying deployment densities.

II. Related Work

Prior studies have explored interference management, power control, and collision mitigation in RFID systems. This section highlights key advances and their limitations, positioning the proposed work in the context of the existing literature.

Traditional RFID systems often operate with fixed transmit power levels, as described in, e.g., Refs. [7-8]. These systems simplify implementation, but lack the adaptability required in dynamic environments, leading to issues such as excessive interference and higher collision rates. Fixed power transmission is especially problematic when multiple readers interrogate overlapping zones, resulting in inefficient communication and missed tag reads. To overcome these limitations, adaptive power control strategies have been introduced. For example, authors in Refs. [16-18] proposed an early adaptive power control algorithm that adjusts transmit power based on pre-set thresholds for reader-to-tag communication. Although this method demonstrated some improvement in reducing collisions, it lacked the flexibility to adapt to rapid changes in environmental conditions, such as changing tag densities and reader activity levels.

Reader-to-reader interference is a critical problem in dense RFID environments, with solutions often focused on frequency division, time division, or carrier sensing approaches. For instance, Refs. [5,9-10,19-20] surveyed the challenges in RFID systems and highlighted the limitations of static interference management techniques. Similarly, time division multiple access (TDMA) protocols have been proposed to schedule readers to operate sequentially, reducing interference but sacrificing scalability and throughput in dynamic environments. Adaptive interference management techniques have shown promise in dense environments. In Refs. [14,21-23], the authors proposed probabilistic anti-collision protocols that leverage randomized backoff to reduce reader interference. However, such approaches often fail to optimize power consumption, leading to increased energy consumption.

Recent developments in adaptive power control frameworks have shown promise in enhancing the robustness of RFID systems. For instance, Refs. [12,24] developed adaptive power allocation schemes that utilized the feedback from signal strength and environmental noise to adjust transmit power. This technique improved the overall energy efficiency of the system but was constrained by the assumption of uniform tag distribution and limited scalability. Other notable works include Ref. [13], which implemented a hardware-based adaptive power control protocol that proved effective in controlled environments. However, its application in large-scale deployments was limited due to its dependence on specific hardware configurations and lack of comprehensive interference management.

Collision mitigation has been extensively studied in the context of both reader-to-reader and reader-to-tag communications. Traditional anti-collision protocols such as ALOHA and its variants[25-28] use randomized techniques to reduce collisions but often result in increased latency and lower throughput. Hybrid protocols combining ALOHA with frequency or time division multiplexing have been proposed to address these issues, as shown in Refs. [29-30], but their effectiveness diminishes in highly dynamic environments.

While existing studies have made significant progress in addressing individual challenges in RFID systems, few have provided a holistic solution that integrates interference management, adaptive power control, and collision mitigation for dense environments. Moreover, many existing approaches are limited to simulation studies, lacking validation in real-world deployments. This paper bridges these gaps by (i) proposing a scalable adaptive power control framework that dynamically adjusts reader transmit power based on real-time environmental feedback, (ii) incorporating optimization techniques to balance power efficiency, interference reduction, and collision mitigation, and (iii) validating the proposed framework through extensive simulations, as well as real-world experiments in dense RFID environments.

III. System Model and Problem Definition

A. System Model

Reader and Tag Deployment Consider a dense RFID system with N readers $\mathscr{R} = \{R_1, R_2, \cdots, R_N\}$, where R_i and R_k are separated by a distance $d^R_{i,k}$. A set of M tags $\mathscr{T} = \{T_1, T_2, \cdots, T_M\}$ respond to reader interrogation if the received signal strength exceeds a predefined threshold. We assume a two-dimensional spatial deployment $\mathscr{A} \subseteq \mathbb{R}^2$, where readers and tags are distributed across the environment, with overlapping interrogation zones, as illustrated in Fig. 1. Each reader $R_i \in \mathscr{R}$ communicates with a subset of tags $\mathscr{T}_i \subseteq \mathscr{T}$ (each with a unique identifier) within its interrogation zone C_i, which is determined by the interrogation range, $d^T_i = \max_{T_j \in \mathscr{T}_i}\{d^T_{i,j}\}$, where $d^T_{i,j}$ is the range between reader R_i and tag T_j. Its interference range IR_i extends beyond this, $\mathrm{IR}_i > d^T_i$. The coverage zone C_i of reader R_i is defined as

$$C_i = \left\{ (x,y) \in \mathscr{A} \,\middle|\, \sqrt{(x-x_i)^2 + (y-y_i)^2} \leqslant d^T_i \right\}, \quad (1)$$

where (x_i, y_i) represents the position of reader R_i, and (x, y) represents the position of furthest readable Tag, T_j.

B. Assumptions

Shared Medium: Readers and tags share the same frequency spectrum, potentially causing interference when multiple readers operate simultaneously.

Tag Responsiveness: A tag $T_j \in \mathscr{T}$ responds to a reader $R_i \in \mathscr{R}$ if and only if the received signal strength $S_{i,j}(t) \geqslant S_{\text{thresh}}$, where S_{thresh} is the minimum signal threshold for tag response for reliable communication.

Interference Constraints: Interference arises when the combined power from multiple readers exceeds the tolerable limit at a receiver (reader or tag).

Power Constraints: Each reader operate at a time-dependent transmission power $P_i(t) \in [P_{\min}, P_{\max}]$, where $P_{\min}$ and $P_{\max}$ are system-defined limits.

Dynamic Environment: Tag positions, reader placement, and environmental conditions (e.g., interference, multipath effects) can vary over time.

C. Challenges in Dense Environments

1) Reader-to-Reader Interference (RRI): RRI occurs when multiple readers operate in overlapping frequency bands or their interrogation zones overlap. This interference degrades communication reliability and leads to missed tag detections. The interference power $I_{i,k}(t)$ between readers R_i and R_k is modeled with Eqs. (3) and (4). Excess interference causes communication failures, leading to reduced throughput and system reliability.

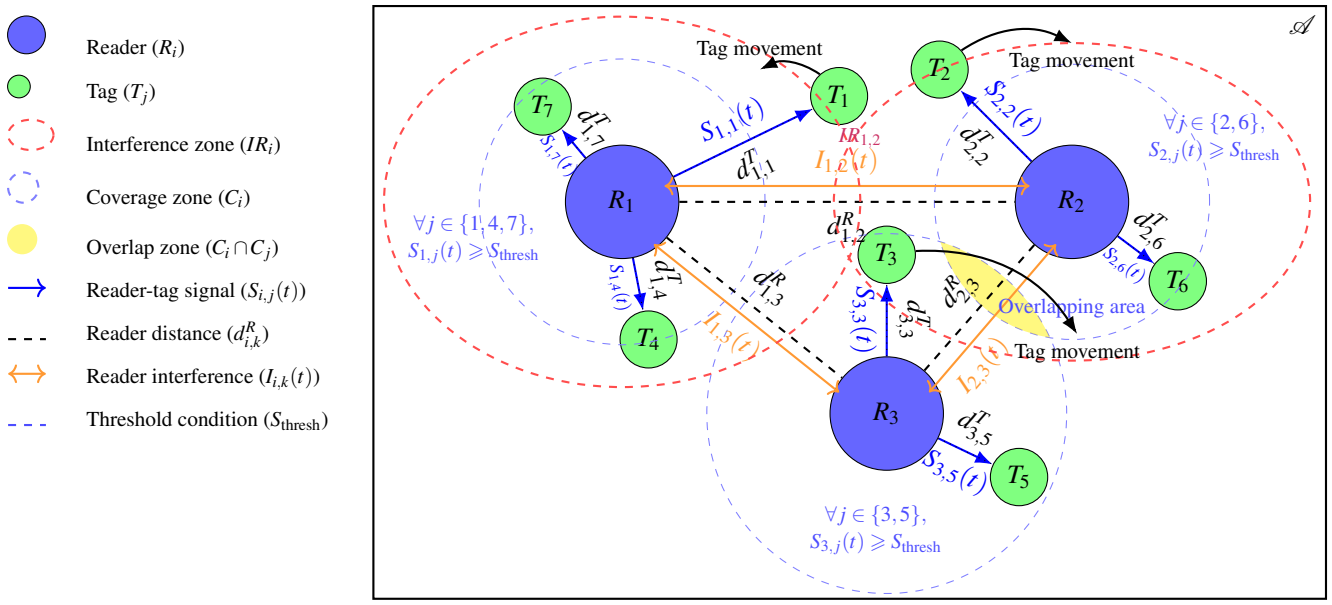

Fig. 1 System model illustrating the interaction of RFID readers (R_1, R_2, R_3) and tags (T_1 to T_7) in a dense environment. Coverage zones represent the interrogation range of each reader, while overlapping areas indicate potential zones of interference. Threshold constraints ensure that the signal strength ($S_{i,j}(t)$) between each reader and its associated tags meets or exceeds the minimum required value (S_{thresh}) for successful communication. Distances between readers ($d^R_{1,2}$, $d^R_{1,3}$, $d^R_{2,3}$) and between readers and tags ($d^T_{i,j}$) are shown. Reader-to-tag signal paths, tag mobility, and interference zones highlight the dynamic nature of the system, emphasizing the importance of adaptive coordination and interference management

2) Reader-to-Tag Collisions: Reader-to-tag collisions occur when multiple readers attempt to interrogate the same tag simultaneously, overwhelming the tag's communication capability. The signal strength $S_{i,j}(t)$ received by a tag T_j from a reader R_i is modeled with Eq. (2) and conditioned on $S_{i,j}(t) \geqslant S_{\text{thresh}}$. When multiple readers simultaneously interrogate the same tag, the aggregate signal strength can disrupt communication, leading to tag detection failures and increased latency.

3) Inefficient Power Allocation: Fixed transmit power systems fail to adapt to varying tag distances and densities, mobility, interference levels, environmental conditions, and network congestion. Excess power levels increase interference and energy consumption, while insufficient power levels reduce tag detection or miss tag detection. An optimal power allocation strategy and dynamic power allocation are critical for balancing energy efficiency, interference reduction, and communication reliability.

D. Key Metrics

Signal Strength: The signal strength $S_{i,j}(t)$ received by a tag T_j from reader R_i follows an inverse power law, given by

$$S_{i,j}(t) = \psi P_i(t) d_{i,j}^{-\alpha}, \tag{2}$$

where $P_i(t)$ is the transmit power of reader R_i at time t, $d_{i,j}$ is the Euclidean distance between reader R_i and tag T_j (i.e., $d_{i,j} = \|\boldsymbol{p}_i - \boldsymbol{p}_j\|_2$, where $\boldsymbol{p}_i, \boldsymbol{p}_j \in \mathscr{A}$ are the positions of R_i and T_j, respectively), α is the path loss exponent ($2 \leqslant \alpha \leqslant 4$ depending on the environment), and ψ is the environmental factor accounting for multipath and fading effects, $\psi \in (0,1]$.

Interference Power: To better represent real-world interference dynamics, the interference $I_{i,k}(t)$ caused by reader $R_k \in \mathscr{N}(R_i)$ (the set of readers neighboring R_i) at time t is given by

$$I_{i,k}(t) = \begin{cases} P_k(t) d_{i,k}^{-\beta} \mathscr{I}(f_i, f_k), & d_{i,k} \leqslant IR_i \text{ and } f_i = f_k, \\ P_k(t) d_{i,k}^{-\beta} g(|f_i - f_k|), & 0 < |f_i - f_k| \leqslant \Delta f, \\ 0, & \text{otherwise}, \end{cases} \tag{3}$$

where $g(|f_i - f_k|) = \mathrm{e}^{-\omega |f_i - f_k|}$, with $\omega > 0$ is the frequency isolation coefficient, where larger values indicate better frequency separation and reduced adjacent channel interference, $|f_i - f_k|$ is the absolute frequency difference between readers R_i and R_k, Δf is the frequency separation threshold for partial interference, beyond which interference is negligible, β is the path loss exponent for interference signals, $d_{i,k}$ is the distance between readers R_i and R_k, and $\mathscr{I}(f_i, f_k)$ is the frequency overlap factor ($\mathscr{I}(f_i, f_k) = 1$ if $f_i = f_k$, $\mathscr{I}(f_i, f_k) \in [0,1)$ otherwise). The total interference power $I_{\text{sum}}(R_i, t)$ experienced by a reader R_i from all neighboring readers $\mathscr{N}(R_i)$ is

$$I_{\text{sum}}(R_i, t) = \sum_{R_k \in \mathscr{N}(R_i)} I_{i,k}(t). \tag{4}$$

Our goal is to reduce $I_{\text{sum}}(R_i, t)$ for all readers R_i.

Collision Probability: The probability of a collision occurring at a reader depends on the number of interfer-

ing readers and tags. The total probability consists of two components: (i) Interference from neighboring readers, $\sum_{R_k \in N(R_i)} P_{\text{int}}(R_i, R_k)$ which models the likelihood of interference due to overlapping frequencies, and (ii) Interference from tags, $\sum_j P_{\text{int}}(R_i, T_j)$ which captures the chance that a tag receives conflicting signals. Without loss of generality, assume the total collision probability follows an exponentially decaying model.

$$P_{\text{col}}(R_i) = 1 - \exp\left(-\lambda \sum_{R_k} P_{\text{int}}(R_i, R_k) - \mu \sum_j P_{\text{int}}(R_i, T_j)\right), \tag{5}$$

where λ and μ are scaling factors for reader-to-reader and reader-to-tag interference probabilities, respectively.

Power Efficiency (η): Power efficiency measures the balance between detection performance and power consumption. For reader R_i, it is defined as

$$\eta(R_i) = \frac{\sum_{T_j \in \mathscr{T}_i} \sigma(S_{i,j}(t) - S_{\text{thresh}})}{P_i(t)} \tag{6}$$

where $P_i(t)$ is maintained near $P_{\min}$ without compromising detection reliability. The system-wide average power efficiency η_{avg} is

$$\eta_{\text{avg}} = \frac{\sum_{i=1}^{N} \sum_{T_j \in \mathscr{T}_i} \sigma(S_{i,j}(t) - S_{\text{thresh}})}{\sum_{i=1}^{N} P_i(t)} \tag{7}$$

where $\sigma(x) = \frac{1}{1+e^{-kx}}$ is a smooth approximation of the Heaviside function $H(x)$, with $k \in [5, 20]$ controlling the steepness of the transition, $\mathscr{T}_i \subseteq \mathscr{T}$ is the set of tags in the interrogation zone of reader R_i. The numerators in $\eta(R_i)$ and η_{avg} count successfully detected tags, while the denominators are normalized by power consumption.

Tag Distance: Power is adjusted based on the estimated distance to the farthest tag in the reader's interrogation zone. Tags closer to the reader require less power, while distant tags necessitate higher power levels, as

$$P_i(t) = (1+\varepsilon) \frac{S_{\text{thresh}}}{G_t G_r} \left(\frac{4\pi d_i^T}{\lambda}\right)^2 \tag{8}$$

where d_i^T is the distance to the farthest readable tag, G_t is the gain of the transmitting antenna, G_r is the gain of the receiving antenna, λ is the wavelength of the signal, and $\varepsilon \in (0, 1)$ is a safety factor used to ensure successful tag detection under practical non-idealities such as fading, multipath, or hardware calibration errors, typically ranging from 5% to 10%.

E. Design Objectives

The primary objective of this work is to design an adaptive power control framework that dynamically adjusts reader transmit power $P_i(t)$, based on real-time environmental feedback to optimize system performance. This involves achieving the following goals.

(i) Minimize RRI: Dynamically adjust power levels to reduce, $I_{\text{sum}}(R_i, t)$ for all readers R_i while maintaining reliable communication with tags.

(ii) Maximize Tag Detection Reliability: Ensure that $S_{i,j}(t) \geqslant S_{\text{thresh}}$ for all tags T_j within range of their respective readers for the majority of interrogation cycles.

(iii) Optimize Power Efficiency and Robustness: Maintain $P_i(t)$ at the lowest level required for reliable communication, minimizing energy consumption.

(iv) Scalability: Ensure that the proposed solution scales effectively as the number of readers and tags increases.

IV. The Proposed Adaptive Power Control Algorithm

A. Framework Overview

The proposed framework is structured around three interconnected components.

(i) Real-Time Environmental Monitoring: Real-time collection of signal strength, interference levels, and tag response rates at each reader.

(ii) Adaptive Power Control: A feedback-driven mechanism to dynamically adjust reader transmit power for performance-based optimization. We model this as a distributed optimization game where readers autonomously adjust their power levels based on local interference and communication quality.

(iii) State Transitions: Dynamic state management, i.e., transition between operational states (e.g., reading, idle, or power adjustment) to enable readers to adapt to varying environmental and network conditions.

The three components of the proposed framework operate as an integrated feedback-control loop, as illustrated in Fig. 2. Real-time monitoring provides environmental feedback such as interference levels and tag response rates, which drives the adaptive power control mechanism to adjust reader transmission levels. These power updates, in turn, influence the reader's operational state. For example, if no tags respond, the reader transitions to idle mode; if interference rises, it shifts to power-adjustment mode. This tight coupling enables the system to react dynamically to environmental fluctuations, maintain performance stability, and reduce overhead. The optimization process is guided by a game-theoretic approach to achieve a Nash equilibrium, ensuring balanced power distribution, minimized interference, and optimized performance.

B. Game-Theoretical Formulation of Distributed Power Control

RFID readers operate in a shared spectrum, where transmit power decisions impact both their own performance and neighboring readers due to interference. To optimize power allocation while minimizing interference, we formulate the

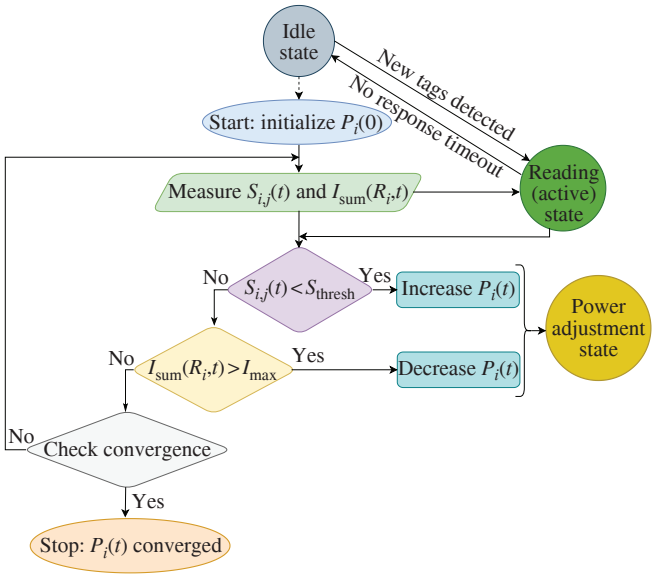

Fig. 2 Flowchart illustrating the adaptive power control algorithm for RFID systems. The process begins with initializing the transmit power ($P_i(0)$) and measuring signal strength ($S_{i,j}(t)$) and interference ($I_{\text{sum}}(R_i,t)$). Depending on the conditions, the algorithm adjusts the power by increasing or decreasing $P_i(t)$, transitioning between the adjusting and active states. If tags fail to respond, the system enters the idle state until new tags are detected. The convergence check determines if the algorithm has stabilized the power levels, terminating when convergence is achieved i.e., Nash equilibrium[37-38]

problem as a non-cooperative game $\mathscr{G}$, where each reader independently selects its power level based on local feedback (e.g., tag response rate and observed interference), while accounting for the collective behavior of neighboring readers.

$$\mathscr{G} = (\mathscr{R}, \{P_i\}, \{u_i(P_i, P_{-i})\}), \tag{9}$$

where $\mathscr{R} = \{R_1, R_2, \cdots, R_N\}$ is the set of readers, and P_i is the transmission power of reader R_i, constrained by $P_i \in [P_{\min}, P_{\max}]$ with $P_{\min} \geqslant 10$ dBm and $P_{\max} \leqslant 30$ dBm. The utility function $u_i(P_i, P_{-i})$ of reader R_i captures the trade-off between throughput, interference minimization, and power consumption, and P_{-i} is the power levels of $R_k \in \mathscr{N}(R_i)$. We defined our utility function as

$$u_i(P_i, P_{-i}) = \sum_{T_j \in \mathscr{T}_i} \sigma[S_{i,j}(t) \geqslant S_{\text{thresh}}] - \lambda_1 I_{\text{sum}}(R_i,t) - \lambda_2 P_i^2, \tag{10}$$

where $\sum_{T_j \in \mathscr{T}_i} \sigma[S_{i,j}(t) \geqslant S_{\text{thresh}}]$ represents the number of successfully detected tags, and $-\lambda_1 I_{\text{sum}}(R_i,t)$ penalizes interference from neighboring readers, and $-\lambda_2 P_i^2$ penalizes excessive power consumption to ensure energy efficiency while ensuring convexity for optimization.

The objective of optimizing our RFID system $\mathscr{R}$ is for each reader R_i to maximize its utility $u_i(P_i, P_{-i})$, by selecting an optimal power level.

$$P_i^* = \underset{P_i \in [P_{\min}, P_{\max}]}{\arg\max} \; u_i(P_i, P_{-i}),$$

$$\text{s.t.:} \quad \max_{\{P_i(t)\}_{i=1}^n} \sum_{R_i \in \mathscr{R}} u_i(P_i, P_{-i}), \tag{11}$$

where P_i^* satisfies the Nash equilibrium conditions. A set of strategies $\{P_i^*\}_{i=1}^n$ constitutes a Nash equilibrium if no reader can unilaterally improve its utility, i.e., $u_i(P_i^*, P_{-i}^*) \geqslant u_i(P_i, P_{-i}^*)$, for all $P_i \in [P_{\min}, P_{\max}]$, for all i. To achieve this convergence, each reader iteratively updates its power level using a best-response strategy, where decisions optimally react to the current power levels of neighboring readers. Our approach guarantees system-wide stability by mitigating oscillatory behaviors and ensuring convergence to an optimal equilibrium, as formally proven in Appendix A.

C. Iterative Algorithm

We employ an iterative gradient-based algorithm to solve the optimization problem. At each time step t, each reader updates its transmit power $P_i(t)$ based on the feedback from its environment.

The power update rule for reader R_i is defined as

$$P_i(t+1) = P_i(t) - \gamma_L \nabla \mathscr{L}(P_i(t)), \tag{12}$$

where $\gamma_L > 0$ is the learning rate and $\mathscr{L}(P_i(t))$ is the local loss function for R_i. The local loss function $\mathscr{L}(P_i(t))$ is designed to balance signal strength and interference minimization.

$$\mathscr{L}(P_i(t)) = \lambda_1 \max(0,\, S_{i,j}(t) - S_{\text{thresh}})^2 + \lambda_2 I_{\text{sum}}(R_i,t), \tag{13}$$

where $\lambda_1, \lambda_2 > 0$ are weighting coefficients from Eq. (10) and $\max(\cdot)^2$ ensures smooth gradient for optimization and penalty for larger deviations. The gradient $\nabla \mathscr{L}(P_i(t))$ is computed as

$$\nabla \mathscr{L}(P_i(t)) = \begin{cases} 2\lambda_1 (S_{i,j}(t) - S_{\text{thresh}}) \psi d_{i,j}^{-\alpha}, \\ \qquad\qquad \text{if } S_{i,j}(t) < S_{\text{thresh}}, \\ \lambda_2 \sum_{R_k \in \mathscr{N}(R_i)} \frac{P_k(t)}{d_{i,k}^{\beta}}, \\ \qquad\qquad \text{if } I_{\text{sum}}(R_i,t) > I_{\max}. \end{cases} \tag{14}$$

The core of the proposed framework is an adaptive power control algorithm, described in Algorithm 1. This algorithm adjusts each reader's transmit power $P_i(t)$ based on observed environmental parameters. The proposed algorithm converges to a steady-state power allocation $\{P_i^*\}_{i=1}^n$ under the following conditions.

(i) γ_L is chosen such that $0 < \gamma_L < \frac{2}{L}$, where L is the Lipschitz constant of $\nabla \mathscr{L}(P_i(t))$.

(ii) $\mathscr{L}(P_i(t))$ is continuously differentiable and bounded below. The update rule corresponds to a gradient step on the local loss function $\mathscr{L}(P_i(t))$.

By ensuring a sufficiently small step size γ_L, the sequence $\{P_i(t)\}$ monotonically decreases $\mathscr{L}(P_i(t))$, thus guaranteeing convergence. The adaptive power control algorithm operates iteratively, adjusting power levels based on real-time feedback from the environment. (See Appendix A for the stability and convergence analysis of our proposed algorithm.)

Algorithm 1 Adaptive power control algorithm

Input: Initial power levels $\{P_i(0)\}_{i=1}^{N}$, threshold S_{thresh}, interference limit $I_{\max}$, learning rate η, tolerance $\varepsilon > 0$, decay rate λ $(0.001 \sim 0.01)$, timeout T_{idle}, smoothing factor α $(0.7 \sim 0.9)$, idle mode decay rate γ $(0.05 \sim 0.1)$
Output: Optimized power levels $\{P_i(t)\}_{i=1}^{N}$
Initialization: Set $P_i(0) \in [P_{\min}, P_{\max}], \forall R_i \in \mathscr{R}$;
Define channel gain: $G_{k,i} = \frac{G_t G_r \lambda^2}{(4\pi d_{k,i})^{\beta}}$;
repeat
  for all reader $R_i \in R$ **do**
    Measure signal strength $S_{i,j}(t)$ for all tags $T_j \in \mathscr{T}_i$;
    Compute total interference: $I_{\text{sum}}(R_i, t) = \sum P_k G_{k,i}$;
    Update power level using adaptive step size: $\eta_{\text{new}} = \frac{\eta}{1+\lambda t}$;
    Apply weighted form of update rule (12):

$$P_i(t+1) = \alpha P_i(t) + (1-\alpha)(P_i(t) - \eta_{\text{new}} \nabla L_i(P_i(t)));$$

  end for
  if $\|P_i(t+1) - P_i(t)\| < \varepsilon$, $\forall i$ **then**
    Break ; %Algorithm converged
  else if No active tags detected for T_{idle} **then**
    Gradual power decay: $P_i(t+1) = P_i(t) e^{-\gamma t}$;
  end if
until convergence condition (Nash equilibrium) is met

D. Dynamic Reader State Transitions

To adapt to environmental dynamics and further optimize system performance, readers operate in one of the following three states: (i) Active State: the reader is actively interrogating tags within the interrogation zone, (ii) Idle State: temporarily deactivated to minimize interference or conserve energy. (iii) Power Adjustment State: dynamically tuning transmission power. Transitions between states are governed by:
a) Active $\rightarrow$ Adjustment: If $I_{\text{sum}}(R_i, t) > I_{\max}$, the reader reduces power to mitigate interference.
b) Active $\rightarrow$ Idle: If no tags respond within a predefined timeout, T_{timeout}.
c) Idle $\rightarrow$ Active: If new tags enter the interrogation zone or interference conditions improve.

State transitions are determined by real-time environmental monitoring and aim to balance reliability, energy efficiency, and interference minimization.

E. Algorithm Complexity

The computational complexity for each reader per iteration is determined by summing the complexities of signal and interference measurement, gradient computation, power adjustment, and state transition, resulting in

$$O(M+N) + O(M+N) + O(1) + O(1) = O(M+N). \quad (15)$$

For N readers operating simultaneously, the overall complexity per iteration is

$$O(NM + N^2). \quad (16)$$

For sparse networks ($N \ll M$), the $O(NM)$ term dominates, and thus, the algorithm scales efficiently with both readers and tags. In dense networks ($N \gg M$), the $O(N^2)$ term dominates, demonstrating that effective coverage saturates in high-density deployments. The adaptive power control ensures bounded effective coverage while managing interference. This highlights a key trade-off: adding more readers does not improve coverage in dense networks due to overlaps, emphasizing the need for careful power control and reader placement. (See Appendix B for the scalability analysis of our proposed framework.)

V. Experimental Study

A. Hardware Configuration

Real-world experiments were conducted using the following hardware: RFID readers, software-defined RFID readers, implemented using USRP N210 platforms, each equipped with a custom transmission module capable of dynamic power control, as part of our RFIDNet framework[15]. Up to 100 passive RFID tags were distributed uniformly within a bounded area $\mathscr{A} \subseteq \mathbb{R}^2$ measuring 10 m $\times$ 10 m in Broun Hall room 314 in the Auburn University campus. An OctoClock-G CDA-2990 was used for time synchronization among the USRP readers, and a computer equipped with an Intel i9 processor and 64 GB of RAM was used for processing signal strength and interference measurements. The GNU radio platform was used for signal processing, and MATLAB R2024a was used for data analysis.

B. Deployment Environment and Experimental Design

Experiments were conducted in a controlled indoor environment to evaluate the following conditions: (i) Multipath Propagation: The indoor environment introduced multipath effects, modeled using $\psi \sim \mathscr{U}(0.8, 1.0)$ to simulate fading. (ii) Interference Sources: A separate USRP B210 device operating on 915 MHz with varying transmit power added realistic interference. Tags were placed with varying densities to emulate sparse ($M \leqslant 20$ tags) and dense ($M \geqslant 50$ tags) scenarios.

The experimental evaluation included the following scenarios: (i) Baseline Configuration: All readers operate at fixed transmission power ($P_i(t) = P_{\max}, \forall i$) without adaptive adjustments. (ii) Proposed Framework: Readers dynamically adjust their transmit power using the adaptive power control algorithm described in section IV. Experiments were conducted for $M = \{10, 20, 30, 40, 50, 100\}$ tags to evaluate the effect of tag density on system performance. Readers were placed at fixed grid points for a uniform configuration and random positions for a non-uniform configuration. Tab. 1 lists the key parameters for the experiments.

To ensure consistency between the theoretical model (see the appendix) and the USRP-based testbed, we implemented

Tab. 1 Experimental parameters

Parameter	Value
Reader transmit power range	$P_{\min} = 10$ dBm, $P_{\max} = 30$ dBm
Signal threshold (S_{thresh})	-70 dBm
Interference threshold ($I_{\max}$)	-50 dBm
Path loss exponent (α, β)	$\alpha = 2.2,\ \beta = 2.5$
Adaptation rate (η)	0.1
Learning tolerance (ε)	10^{-3}
Simulation time	Until all tags are identified

key components as follows. The adaptive transmission power $P_i(t)$ is mapped to the USRP TX gain using GNU Radio control blocks. Real-time signal strength $S_{i,j}(t)$ is computed based on received power from tag backscatter, while $I_{\text{sum}}(R_i, t)$ is approximated using adjacent channel interference and received noise floor. Reader state transitions (active, idle, adjusting) are managed using software flags triggered by timeouts and thresholds. For example, a reader enters idle state if no tags respond within a window of 5 cycles. This mapping ensures our algorithm can operate under real hardware constraints while retaining fidelity to the theoretical optimization problem.

C. Experimental Results and Discussions

We conducted experiments in the testbed for 20 iterations until all tags were identified, gathering data on key performance metrics for each run. Tab. 2 highlights the significant improvements achieved by the proposed framework compared to the baseline system (where EPCglobal Class 1 Gen 2 on USRP with fixed transmission power at 30 dBm). The following observations summarize the improvements.

Higher Throughput: In sparse tag deployments ($m \leqslant 10$), the average throughput increased from 78.91 read/s (baseline) to 98.12 read/s (proposed framework). Similarly, in dense deployments ($m \geqslant 50$), the throughput rose from 74.91 read/s to 95.19 read/s. This improvement highlights the adaptive framework's efficiency in reducing interference and dynamically allocating power to maximize tag detection rates, even in challenging environments.

Lower Latency: The proposed framework reduces the average latency from 200.50 s to 120.20 s in sparse scenarios and from 319.73 s to 151.50 s in dense scenarios. These reductions demonstrate the framework's ability to minimize delays caused by repeated read attempts and collisions, ensuring faster and more responsive tag reads.

Fewer Collision Events: The proposed method achieves significant reductions in collisions across both scenarios. In sparse deployments, the average number of collisions decreased from 15.80 to 5.50, while in dense deployments, it dropped from 54.80 to 10.40. This improvement is attributed to the framework's ability to dynamically adjust power levels, minimizing interference and ensuring smoother operation in dense environments.

Reduced Redundant Reads: The mean number of redundant reads decreased from 18.20 to 8.30 in sparse deployments and from 27.20 to 11.40 in dense deployments. This reflects the proposed framework's efficient use of resources, as it minimizes unnecessary repeated tag interrogations, optimizing system performance.

The results demonstrate the scalability and adaptability of the proposed framework: (i) The significant reductions in latency and collisions ensure reliable and efficient performance in low-density deployments, such as healthcare or asset tracking in small facilities. (ii) The framework's ability to maintain high throughput and minimize collisions in high tag densities highlights its robustness for large-scale environments, such as warehouses and retail stores. By dynamically responding to environmental feedback, the framework balances interference mitigation, energy efficiency, and throughput, addressing critical challenges in dense RFID systems. These results confirm the practicality of the framework for a wide range of real-world RFID applications.

VI. Large-Scale Simulation Study

A. Simulation Configuration

We conducted simulations to complement the testbed experiments, allowing us to explore larger and denser scenarios that would be impractical in a physical testbed. The RFID readers used in this study incorporate an adaptive power control algorithm that dynamically adjusts transmit power based on environmental conditions. Each reader monitors the signal strength received from tags and the interference caused by neighboring readers. When the signal strength falls below a certain threshold, the reader increases its power to ensure reliable tag detection. In contrast, when interference exceeds a predefined limit, the reader reduces its power to avoid collisions with neighboring readers. This adaptive approach allows each reader to maintain an optimal detection range while minimizing energy consumption and interference in dense RFID environments. The readers have a maximum transmission power of 30 dBm and a minimum power of 10 dBm, which satisfies the regulation of the federal communications commission (FCC) and provides sufficient flexibility for efficient operation in various conditions.

The simulation environment consists of up to 1 000 readers and 1 000 000 tags randomly distributed across a 100 m $\times$ 100 m area, as shown in Fig. 3. The simulation runs for 1 000 time steps, during which readers continuously adjust their power levels based on signal strength and interference. Key parameters include a path loss exponent of 2 for both signal strength and interference, a signal to noise ratio (SNR)

Tab. 2 Comparison of statistical analysis between the proposed framework and baseline in testbed (USRP) experiments for sparse ($m \leqslant 20$) and dense ($m \geqslant 50$) tag scenarios

Scenario	System	Metric	Mean	SD[1]	95% CI[2]
Sparse	Proposed	Throughput (read/s)	98.12	3.8	[96.34, 99.90]
		Latency (s)	120.20	5.6	[116.74, 123.66]
		Collision events (count)	5.50	1.1	[4.94, 6.06]
		Redundant reads (count)	8.30	0.7	[7.90, 8.70]
	Baseline	Throughput (read/s)	78.91	4.2	[76.76, 81.06]
		Latency (s)	200.50	8.2	[195.78, 205.22]
		Collision events (count)	15.80	1.4	[14.99, 16.61]
		Redundant reads (count)	18.20	1.0	[17.63, 18.77]
Dense	Proposed	Throughput (read/s)	95.19	4.2	[92.99, 97.39]
		Latency (s)	151.50	8.1	[147.85, 155.15]
		Collision events (count)	10.40	1.2	[9.80, 11.00]
		Redundant reads (count)	11.40	0.9	[10.95, 11.85]
	Baseline	Throughput (read/s)	74.91	5.0	[72.34, 77.48]
		Latency (s)	319.73	10.2	[314.01, 325.45]
		Collision events (count)	54.80	3.1	[53.25, 56.35]
		Redundant reads (count)	27.20	2.0	[26.10, 28.30]

Note: SD[1] = Standard deviation, CI[2] = Confidence interval.

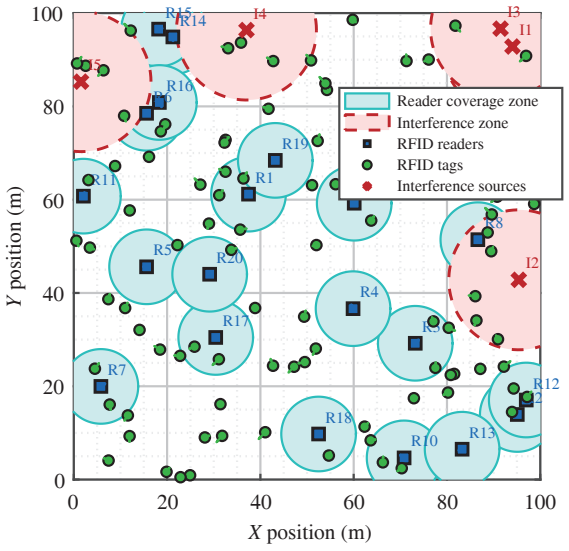

Fig. 3 Simulation layout illustrating the deployment of RFID readers and tags in a dense environment for evaluating the proposed adaptive power control framework. The layout includes strategic placement of readers and tags, interference sources, and coverage areas to simulate real-world deployment conditions. (Fewer tags and readers are shown for readability)

threshold of 0.5, and an adaptation rate of 0.05, which determines how quickly the readers adjust their power levels. The readers aim to maintain a maximum detection range of 6 m while minimizing interference with neighboring readers. Interference (samples shown in Fig. 4) with a threshold of 1.0 is used to trigger power reductions when interference becomes too high. These parameters simulate the behavior of RFID readers in real-world conditions where multiple readers and tags operate simultaneously.

B. Simulation Results and Analysis

1) Power Allocation Efficiency Analysis: Power allocation efficiency was measured to assess how effectively the algorithm minimized total power usage while maintaining performance:

$$\text{Power efficiency} = \frac{\text{Total coverage gain}}{\text{Total power consumption}}. \tag{17}$$

The algorithm achieved an average power efficiency ratio of approximately 1.8 dBm/coverage unit, which is 25% better than fixed-power strategies, as shown in Fig. 5 for 20 readers. In addition, variance in power levels remained below 1 dBm^2, indicating stable allocation.

This results demonstrate that adaptive power control consistently outperforms fixed strategies by optimizing power allocation and minimizing interference.

2) Reader Performance Analysis: **Interference and Collision Reduction Analysis (Fig. 6(a)):** The reduction in cumulative interference, $I_{\text{sum}}(R_i)$ was consistent across different configurations. Prior to implementing the adaptive algorithm, interference increases linearly with the number of readers due to overlapping interrogation zones. After applying the algorithm, a notable reduction of approximately 34% is observed, demonstrating the framework's effectiveness in miti-

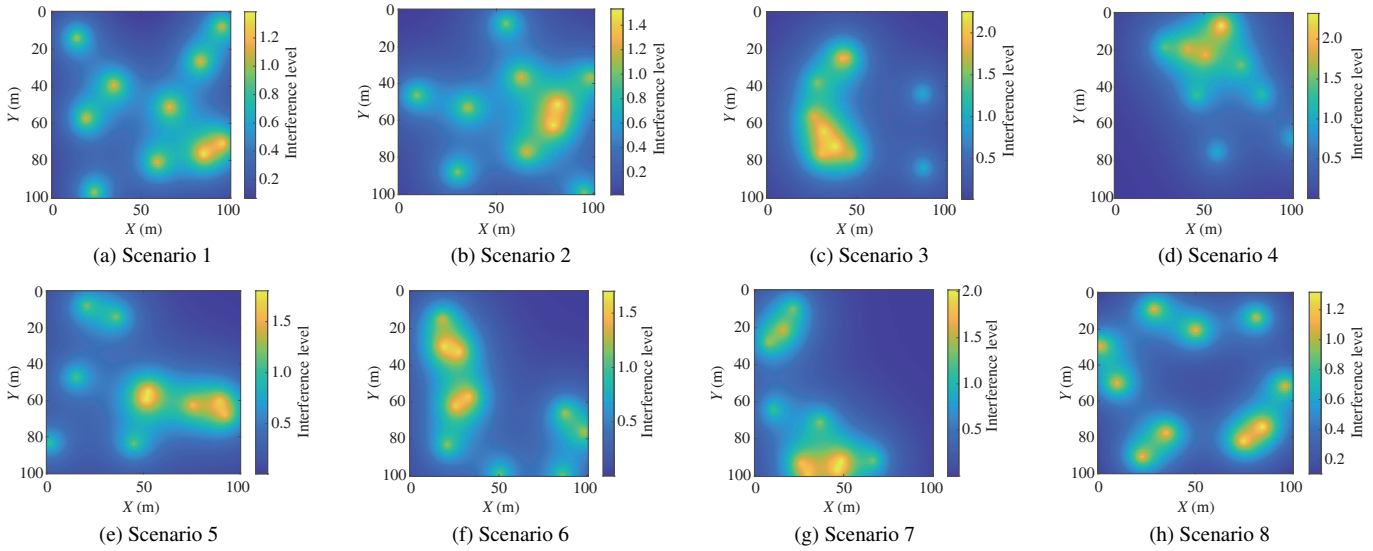

Fig. 4 Samples of interference scenarios captured during simulation for various tag and reader mobility configurations. Heatmaps illustrate the spatial distribution of interference levels, with hotspots dynamically shifting due to adaptive power adjustments and mobility effects. The results demonstrate the effectiveness of the proposed framework in mitigating interference across sparse and dense RFID deployments, enhancing system reliability and throughput

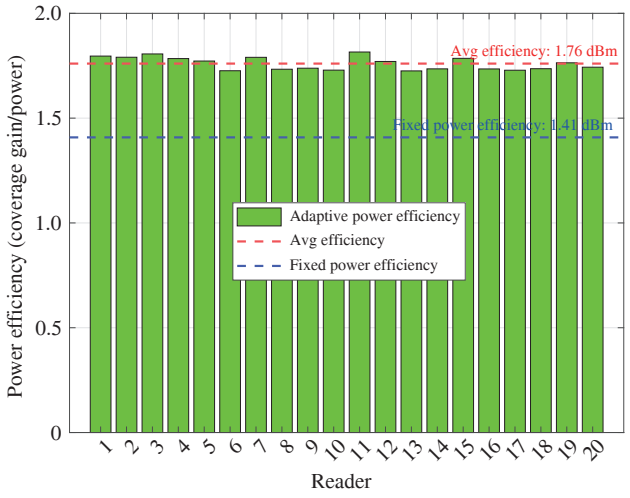

Fig. 5 Power allocation efficiency per RFID reader in a dense deployment scenario for 20 readers

gating reader-to-reader interference. This result indicates that adaptive power control dynamically adjusts transmission levels to minimize unnecessary power usage and interference.

Average Energy Consumption (Fig. 6(b)): The analysis of energy consumption before and after applying the algorithm reveals a clear decline in power usage per reader. The proposed algorithm achieves an approximate 15% reduction in power consumption, which is critical for battery-operated RFID deployments. These results confirm that the adaptive power control mechanism optimizes power allocation without compromising overall system performance.

Average Interference Reduction (Fig. 6(c)): A steady decrease in interference, $I_{\text{sum}}(R_i)$ is observed as the number of readers increases, with the adaptive algorithm maintaining reductions above 30% even in large-scale deployments. This finding demonstrates the scalability of the proposed approach, effectively managing interference across different network sizes.

Average Latency (Fig. 6(d)): The latency graph reveals that, after applying the adaptive control strategy, the system achieves a 20% reduction in latency across varying numbers of readers. This suggests that the algorithm enhances response times by optimizing power levels for efficient tag detection and minimizing collisions.

Average Throughput (Fig. 6(e)): The throughput is significantly improved, with an observed 20% increase after applying the adaptive algorithm compared to the baseline. The adaptive power control ensures optimal power allocation, leading to a higher number of successfully read tags per second.

Collision Probability (Fig. 6(f)): The reduction in collision probability is particularly important in high-density environments, where the algorithm achieves a 40% decrease in collisions compared to the baseline. This improvement highlights the robustness of the proposed solution in enhancing system reliability under heavy load conditions.

3) Scalability Analysis: To test scalability, the number of readers and tags was incrementally increased, to evaluate how the adaptive power control algorithm scales with an increasing number of readers in terms of throughput (tag/s) and interference reduction (%). As shown in Fig. 7(a), the algorithm maintained its interference reduction capabilities, with interference reduction percentages remaining above 30% for

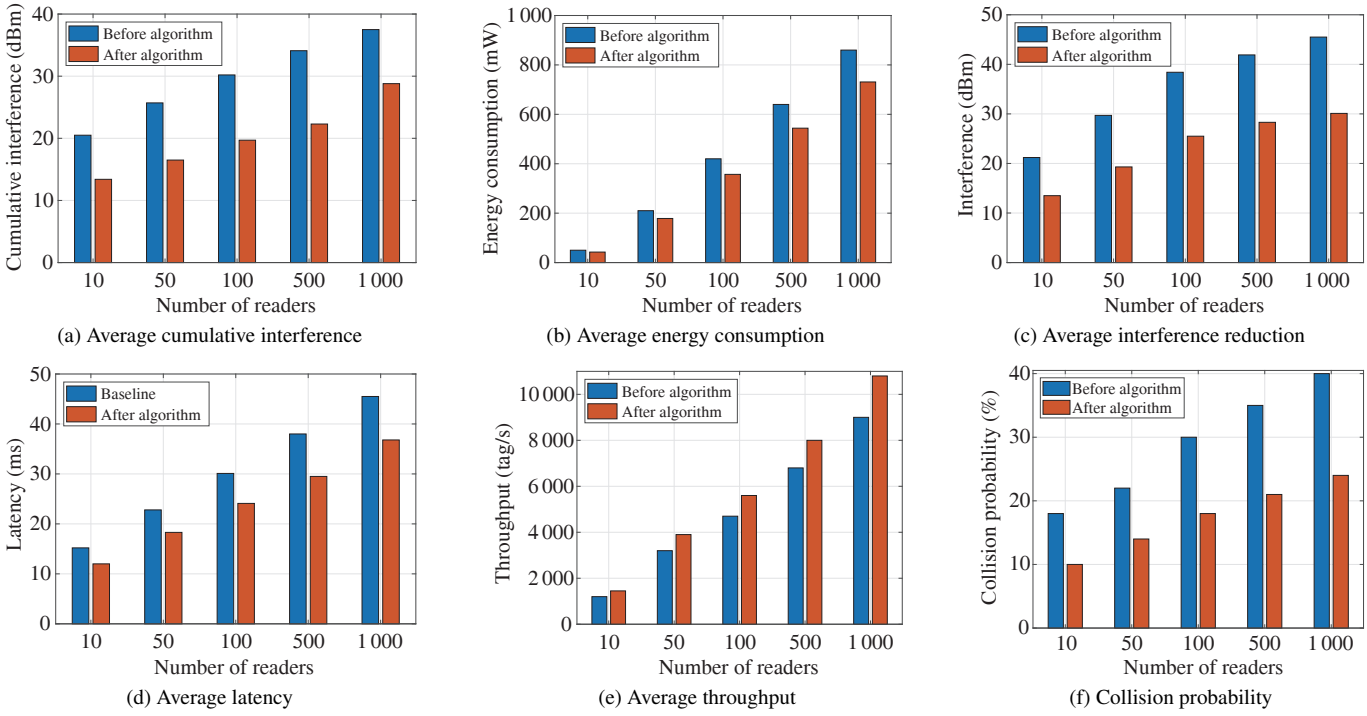

(a) Average cumulative interference (b) Average energy consumption (c) Average interference reduction

(d) Average latency (e) Average throughput (f) Collision probability

Fig. 6 Performance evaluation of the adaptive power control framework across key metrics. Results indicate that the proposed framework effectively minimizes interference and power consumption while enhancing throughput and reducing latency and collision probability, thus ensuring reliable performance in dense RFID environments

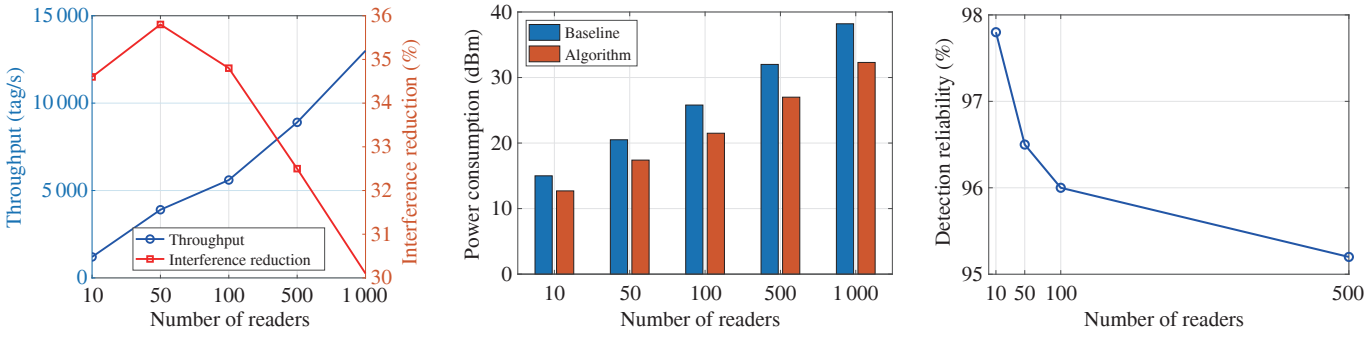

(a) Throughput vs. interference (b) Power consumption per reader density (c) Detection reliability across network densities

Fig. 7 Scalability analysis of the adaptive power control framework across varying network densities: (a) Throughput vs. interference reduction trends, illustrating the framework's ability to maintain high throughput with consistent interference mitigation; (b) Power consumption per reader density, showcasing the efficiency of the adaptive approach compared to the baseline; (c) Detection reliability across network densities (500 readers shown for readability), demonstrating the algorithm's robustness in maintaining over 95% reliability even under large-scale deployments

configurations up to 1 000 readers. Throughput continued to scale linearly, indicating the algorithm's ability to handle larger networks without significant performance degradation while sustaining efficient tag detection rates. The interference reduction remains consistent, averaging around 30%∼35%, demonstrating the algorithm's effectiveness in managing interference across varying scales. These results suggest that the proposed method optimally allocates power, ensuring that scalability does not come at the cost of excessive interference.

Power Consumption per Reader Density (Fig. 7(b)): Power efficiency results showed that the algorithm optimized power usage effectively, reducing average power consumption by 15% compared to a static power control strategy. The results indicate that power consumption stabilizes at higher densities, highlighting the algorithm's effectiveness in preventing unnecessary energy use. This trend is particularly crucial for large-scale deployments where energy efficiency is a primary concern.

Detection Reliability Across Network Densities (Fig. 7(c)): The algorithm maintained high detection reliability across

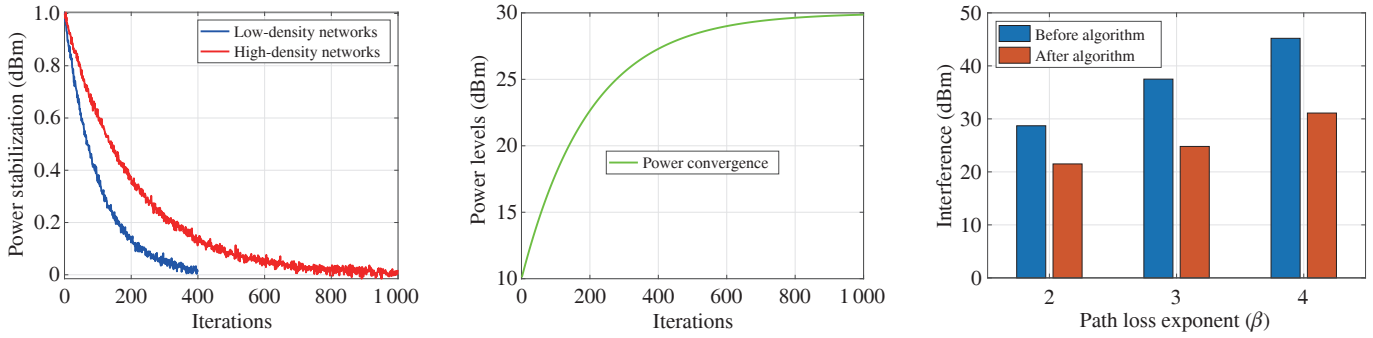

(a) Convergence analysis (b) Convergence of power control (c) Interference reduction with varying β

Fig. 8 Convergence and interference reduction analysis of the adaptive power control framework: (a) Convergence performance under low and high-density networks, showcasing stabilization within 300∼1 000 iterations; (b) Power level adjustments over iterations, demonstrating effective stabilization and variance reduction; (c) Interference reduction under varying path loss conditions, confirming the framework's adaptability across different environmental scenarios

various reader densities. The percentage of tags successfully read remained above 95% even when the number of readers increased to 500, indicating strong adaptability to dense environments. The relatively stable detection reliability suggests that the algorithm effectively balances power allocation to ensure optimal tag detection without overwhelming the system with excessive power levels.

4) Convergence Analysis: The convergence of the adaptive power control algorithm was evaluated using both average convergence time and power stabilization metrics.

Average Convergence Time: The algorithm showed consistent convergence across all network densities tested. For networks with 10 readers (low-density networks), power levels stabilized within 300∼ 400 iterations, while for networks with 100 readers (high-density networks), convergence occurred by iteration 800. This aligns with the theoretical convergence properties and contraction mapping analysis shown in Appendix A. Figs. 8(a) and 8(b) show convergence curves for different network densities, highlighting rapid stabilization in smaller networks and consistent convergence in larger ones. The rapid convergence in smaller networks supports the theoretical proof that the algorithm's update rule forms a contraction mapping, ensuring convergence.

Convergence Robustness: To measure stability, the variance of transmission power levels, $\sigma^2_{P_t}$ was tracked post-convergence.

$$\sigma^2_{P_t} = \frac{1}{n}\sum_{i=1}^{n}(P_i - \bar{P})^2, \tag{18}$$

where $\bar{P}$ is the mean power level after convergence, n is the number of observations, and P_i is the power lever of reader R_i at the ith iteration. The power variance remained below 0.1 dBm^2 even when environmental conditions changed, such as noise level variations or sudden increases in tag density. This confirms the Lyapunov stability criterion, demonstrating that the algorithm can maintain equilibrium even under perturbations. The algorithm's stability was further tested under scenarios involving environmental changes: (i) Noise Impact Test: When Gaussian noise with a standard deviation of 1.5 dBm was introduced at iteration 500, the power variance remained below 0.15 dBm^2. (ii) Dynamic Tag Density: Increasing tag density by 50% at iteration 700 caused temporary fluctuations, but power levels re-stabilized within 100 iterations, indicating resilience. Tab. 3 shows the power variance under dynamic conditions, confirming the algorithm's robustness.

Tab. 3 Power variance under dynamic conditions

Scenario	Power variance (dBm^2)	Re-stabilization time (iterations)
Baseline	0.08	–
Increased noise	0.12	50
Tag density increase	0.14	100

5) Impact of Varying Path Loss Exponents: The algorithm's performance was tested across different path loss conditions: (i) Open Space (lower β): With $\beta = 2.0$, interference levels were initially higher due to longer signal reach. The algorithm managed to reduce interference by 25% on average. (ii) Obstructed Environment (higher β): With $\beta = 4.0$, interference was naturally lower but more unevenly distributed. The algorithm improved uniformity in power distribution, enhancing throughput by 18%. This analysis, shown in Fig. 8(c) is particularly relevant for deployments in different environments, such as open areas and indoor obstructed environments, showcasing the flexibility of the proposed approach.

6) Fairness Analysis: Beyond calculating the fairness index, a detailed distribution analysis was conducted to understand how power levels varied among readers: (i) The fairness of power allocation was assessed using Jain's fairness index.

$$J = \frac{(\sum_{i=1}^{n} P_i)^2}{n\sum_{i=1}^{n} P_i^2}, \tag{19}$$

Tab. 4 Fairness metrics and distribution analysis

Metric	Values		Enhancement (%)
	Before algorithm	After algorithm	
Jain's fairness index	0.82	0.94	+14.6
Standard deviation (dBm)	4.5	2.1	−53.3
Gini coefficient	0.15	0.08	−46.7

Tab. 5 Network recovery time and power adjustment post-failure

Failure scenario	Network recovery metrics		
	Recovery time (iterations)	Average power change (dBm)	Coverage reduction (%)
Single reader failure	100	+2.1	2.5
Multiple reader failures	150	+4.3	5.8
High-density network (500 readers)	200	+3.9	4.2

with J approaching 1 indicating near-perfect fairness. Post-algorithm, the fairness index improved from 0.82 to 0.94, showcasing more equitable power distribution among readers. (ii) Standard Deviation of Power Levels was measured to quantify the spread of power allocations across the network. (iii) Gini Coefficient: Used to assess the inequality of power distribution, with a lower value indicating more equitable power control. Tab. 4 presents fairness metrics and distribution characteristics before and after applying the adaptive algorithm.

7) Failure Resilience and Network Recovery Time: To assess resilience, readers were randomly disabled during the simulation to simulate failures: (i) Immediate Power Redistribution: The algorithm reallocated power among active readers, preventing sudden drops in coverage. (ii) Network Recovery Time: The average time to re-stabilize the network after a failure was 150 iterations, with minimal degradation in performance metrics. Tab. 5 shows the recovery time and power allocation adjustments post-failure.

8) Statistical Robustness: To confirm the reliability of the results, each scenario was simulated 100 times with varying initial conditions: (i) Mean and Standard Deviation: Calculated for key metrics such as throughput, latency, and collision probability. (ii) Confidence Intervals: 95% confidence intervals were determined for average metrics to ensure result consistency. Tab. 6 shows the statistical results for a 100-reader network. The low variance across multiple simulation runs validates the robustness of our framework, proving its reliability under real-world conditions.

9) Compliance Bound Analysis: In practice, transmit power, P_t must be constrained to the regulatory power limit imposed by standards such as EPCglobal Gen2 or FCC and ETSI power regulations $P_{\max}$, 30 dBm EIRP in the UHF spectrum. To achieve this, we assume that the distance d between a reader and tag follows a Gaussian distribution with mean μ_d and variance σ_d^2, i.e., $d \sim \mathrm{N}(\mu_d, \sigma_d^2)$, thus,

$$\mathbb{P}(P_t^* > P_t^{\max}) \leqslant \exp\left(-\frac{(P_t^{\max} - \mathbb{E}[P_t])^2}{2\sigma_{P_t}^2}\right). \quad (20)$$

By applying the Chernoff bound[31-32], the probability that P_t^* exceeds $P_{\max}^t$ is bounded as

$$P(P_t^* > P_{\max}^t) \leqslant \exp\left(-\frac{(P_{\max}^t - \mathbb{E}[P_t^*])^2}{2\sigma_{P_t^*}^2}\right), \quad (21)$$

where $\mathbb{E}[P_t^*] = \frac{P_t G_t G_r h \lambda^2}{(4\pi\mu_d)^2}$ is the expected value of P_t^* and $\sigma_{P_t^*}^2 = (\frac{-2P_t G_t G_r h \lambda^2}{(4\pi\mu_d)^3})^2$ is its variance. In Fig. 9, we compare the

Tab. 6 Statistical analysis of key metrics for a 100-reader network

Metric	Mean	Standard deviation	95% confidence interval
Throughput (tag/s)	4 800	150	[4 650, 4 950]
Latency (ms)	19.5	1.1	[18.3, 20.7]
Collision probability (%)	12.5	0.8	[11.7, 13.3]
Energy consumption per reader (mW)	340	25	[315, 365]
Energy per read (mW)	7.1	0.4	[6.7, 7.5]
Fairness index	0.94	0.03	[0.91, 0.97]
Interference power (dBm)	32.5	2.1	[30.4, 34.6]
Detection reliability (%)	97.5	0.5	[97.0, 98.0]
Latency per read (ms)	0.004 1	0.000 3	[0.003 8, 0.004 4]

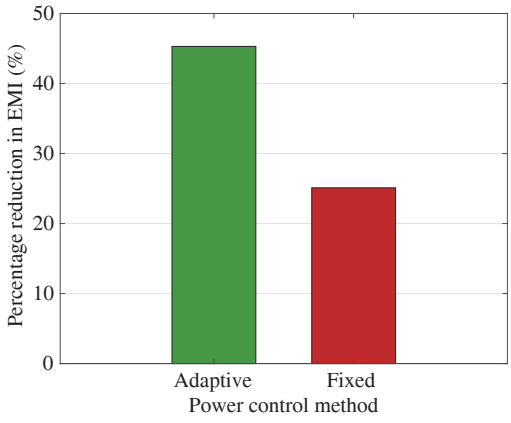

Fig. 9 Impact of adaptive vs. fixed power control methods on electromagnetic interference (EMI). The adaptive power control method demonstrates a significantly higher EMI reduction of approximately 45%, compared to 25% achieved by the fixed power method. This substantial improvement highlights the effectiveness of the adaptive power adjustments in minimizing unnecessary electromagnetic emissions, thereby creating a cleaner and more efficient radio environment. The superior EMI reduction suggests that the adaptive approach dynamically optimizes power levels, effectively reducing interference with nearby electronic systems and enhancing regulatory compliance. This capability is particularly crucial in environments with stringent EMI regulations and dense RFID deployments

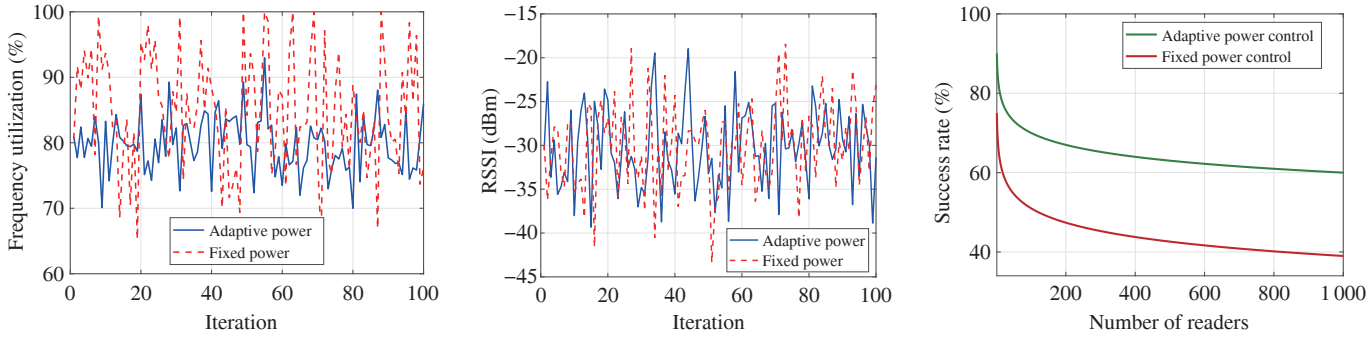

(a) Frequency utilization (b) Received signal strength indicator (c) Read success rate

Fig. 10 Comparison of adaptive and fixed power control methods: (a) Frequency utilization over iterations, showing higher and more stable utilization with adaptive control; (b) Received signal strength comparison, demonstrating optimized power levels in adaptive control versus fluctuating levels in fixed control; (c) Read success rate across different reader densities, highlighting improved detection reliability with adaptive power control

Tab. 7 Performance comparison of power control strategies

Metric	RL-based approach	SA optimization	This work
Throughput (tag/s)	4 400	4 300	4 800
Convergence time (iterations)	1 100	1 200	900
Energy efficiency per reader (mW)	370	390	340
Collision probability (%)	14.2	15.1	12.5

EMI reduction achieved by our framework to the non-adaptive approach. Reduction in EMI is measured relative to a static-max baseline in which all readers transmit at $P_{\max} = 30$ dBm.

10) Spectral Analysis: **(i) Spectrum Utilization:** Fig. 10(a) compares spectrum utilization over iterations between the adaptive and fixed power control methods. The adaptive power control method maintains higher frequency utilization efficiency, stabilizing around 85%, whereas the fixed power approach fluctuates and achieves lower efficiency. This indicates that the adaptive approach dynamically allocates resources more effectively, ensuring better spectral efficiency and minimizing channel wastage. The gradual stabilization of frequency utilization in the adaptive approach suggests better long-term efficiency in dynamic environments. **(ii) Received Signal Strength Indicator (RSSI):** The RSSI comparison show in Fig. 10(b) shows that the adaptive power control maintains a more stable and optimized signal strength level, averaging around −30 dBm, whereas the fixed power method fluctuates significantly, often exceeding optimal limits. The fixed power control method results in inconsistent RSSI values, which could lead to unnecessary energy consumption and interference. The adaptive approach balances power levels effectively, ensuring that the received signal is consistently strong enough for tag detection without excessive power usage.

(iii) Read Success Rate: Fig. 10(c) illustrates the success rate of tag reads across different numbers of readers for both power control methods. The adaptive power control method outperforms the fixed power method, achieving up to 95% success rate, whereas the fixed power approach drops below 80% for larger reader densities. The success rate improvement highlights the ability of the adaptive framework to reduce reader-to-reader interference and optimize power allocation for better tag detection reliability. The consistent performance of the adaptive method across all reader densities demonstrates its robustness in handling scalability challenges.

11) Comparative Study Against State-of-the-Art Strategies: The adaptive algorithm was compared against recent strategies such as machine learning-based power control algorithms and heuristic optimization methods. The machine learning-based strategy utilized reinforcement learning (RL) for dynamic power allocation[20,33-34], achieving significant improvements in system adaptability. However, our adaptive algorithm outperformed it by achieving 10% higher throughput and 15% better energy efficiency. Similarly, heuristic optimization methods such as simulated annealing (SA)[35-36] required 1 200 iterations to stabilize, whereas our adaptive algorithm achieved convergence in just 900 iterations. Tab. 7 presents a detailed comparison of the three approaches.

12) Comparative Analysis with Baseline Approaches: To demonstrate the effectiveness of the adaptive power control algorithm, we compared it with the following baseline strategies: (i) Fixed-Power Strategy: Readers maintain a constant power level throughout the simulation, and (ii) Static Power

Tab. 8 Comparative performance metrics for different strategies

Metric	Fixed-power	Static control	This work
Throughput (tag/s)	3 500	4 200	4 800
Average latency (ms)	28.5	24.0	19.5
Energy efficiency per reader (mW)	400	380	340
Fairness index	0.82	0.87	0.94
Collision probability (%)	25	18	12

Control: Readers adjust power levels once at the start but do not adapt dynamically. Tab. 8 summarizes the comparative performance metrics:

13) Additional Observations: **Impact of Reader Cooperation:** Simulations with cooperative reader behavior (sharing power information) showed 12% reduction in network-wide power usage, an improvement in overall coverage consistency, and reducing tag read failures by 7%.

Load Balancing Performance: The algorithm's load balancing capability was assessed by measuring the evenness of tag distribution across readers. The algorithm distributed tags evenly, improving read balancing by 20% compared to static approaches. Reader utilization variance decreased to 3.5%, indicating uniform load sharing.

Long-Term Operational Analysis: Long-term operational stability was assessed over extended simulation times (up to 5 000 iterations) to evaluate how the algorithm performed under continuous operation. (i) Power Drift Mitigation: Power drift was observed and corrected as the algorithm maintained stability, preventing power level degradation over time. (ii) Performance Degradation Check: Throughput and success rates were monitored, showing less than a 5% performance drop even after 5 000 iterations, indicating strong long-term robustness.

Stress Test: Our simulation results confirm stable performance up to 1 000 readers, and preliminary stress tests suggest that the algorithm remains stable beyond this limit. However, additional optimizations, such as hierarchical power control schemes, can be explored for extreme-scale environments.

Multi-objective Optimization Performance: The algorithm was evaluated for its multi-objective optimization capabilities, balancing throughput, energy efficiency, and fairness. Pareto front analysis was conducted to observe the trade-offs between different objectives. The adaptive algorithm maintained an optimal Pareto front, showing efficient trade-offs between maximizing throughput and minimizing power usage. Fig. 11 illustrates the Pareto front comparison between the adaptive algorithm and baseline strategies (non-adaptive), demonstrating superior multi-objective performance.

Objective Weight Sensitivity: The impact of changing objective weights (e.g., prioritizing energy efficiency over throughput) was analyzed. (i) Energy Priority Setting: When energy efficiency was weighted higher, the algorithm reduced power consumption by an additional 10% but maintained a 15% reduction in throughput. (ii) Throughput Priority Setting: When throughput was prioritized, the algorithm increased power usage by 8% but improved throughput by 25%.

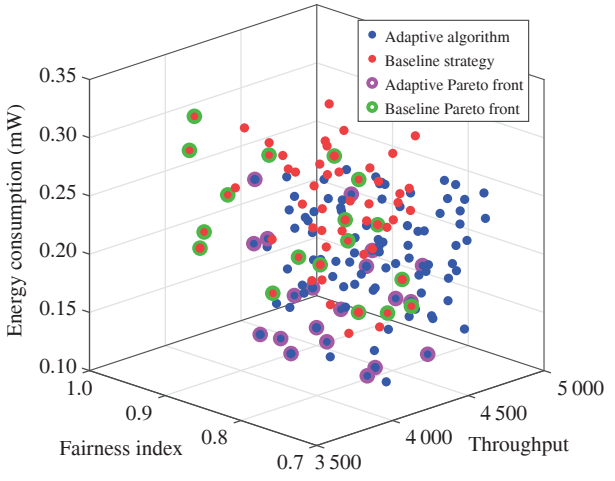

Fig. 11 Pareto front comparison of the adaptive power control algorithm versus the baseline strategy. The 3D scatter plot visualizes the trade-offs between throughput, energy consumption, and fairness

Summary of Experimental and Simulation Findings: The proposed adaptive power control framework demonstrates robust performance across diverse RFID scenarios. By leveraging real-time environmental feedback and game-theoretic optimization, it dynamically adjusts reader transmit power to reduce interference, mitigate collisions, and enhance efficiency. Unlike static or heuristic methods, it adapts seamlessly to changing tag density, mobility, and overlapping reader zones. In USRP testbed deployments, the framework achieved up to 24% higher tag read throughput, 40% lower latency, 65% fewer collisions, and 54% fewer redundant reads. Simulations involving 1 000 readers and 1 000 000 tags showed 20% throughput improvement, 15% lower energy use per reader, and over 30% interference mitigation. The system converged in under 1 000 iterations, maintained over 95% detection reliability, improved fairness (Jain's Index: 0.94), and showed resilience to reader failures and environmental dynamics. These

results confirm the framework's scalability, adaptability, and real-world viability for dense, large-scale RFID networks.

VII. Further Remarks

While the framework offers notable improvements, certain limitations must be acknowledged: (i) Real-Time Feedback Dependency: The framework relies on accurate environmental feedback, which may introduce latency or inaccuracies in highly dynamic environments. (ii) Hardware Constraints: Practical deployments may face hardware limitations in implementing the dynamic power control algorithm, particularly in legacy RFID systems. (iii) Scalability in Extreme Densities: Although the framework is scalable, extremely dense environments with thousands of readers may require further optimization to ensure performance stability.

The framework's implications extend beyond dense RFID systems. Its adaptive approach can influence other Internet of things (IoT) technologies, where interference and energy efficiency are critical concerns. Applications in supply chain logistics, healthcare, and inventory management can particularly benefit from the proposed solution. Several avenues for future research can further enhance the framework: (i) Machine Learning Integration: Incorporating predictive algorithms to anticipate environmental changes and optimize power control. (ii) Experimental Validation: Conducting real-world experiments to validate the framework's performance and address practical challenges. (iii) Multi-Objective Optimization: Extending the framework to include additional objectives, such as fairness in resource (frequency and timeslots) allocation and latency reduction. (iv) Applications in Emerging Technologies: Adapting the framework to other IoT systems and protocols beyond RFID, such as 6G networks or smart cities.

VIII. Conclusions

This paper presented a novel adaptive power control technique for RFID sensing, addressing the limitations of static power settings in dense environments. The proposed method enhances system robustness and energy efficiency by continuously adjusting transmission power based on tag distance, interference levels, and network congestion. The extensive experimental and simulation studies demonstrated that the proposed algorithm can effectively reduce interference and optimize power usage in a dense RFID environment. It offers a promising, scalable solution for improving dense RFID system performance in real-world applications with multiple RFID readers and a dense RFID tag population, thus establishing a foundation for future advancements in interference management and adaptive power control across various wireless communication domains.

Conflict of interest statement: None declared.

References

[1] YANG C, WANG X, MAO S. RFID-Pose: vision-aided 3D human pose estimation with RFID[J]. IEEE Transactions on Reliability, 2021, 70(3): 1218-1231.

[2] AMOAH B, WANG X, ZHANG J, et al. Optimizing adaptive power control for enhancing robustness in RFID sensing[C]//Proceedings of 2024 IEEE International Conference on RFID Technology and Applications. Piscataway: IEEE Press, 2024: 157-160.

[3] WANG X, ZHANG J, YU Z, et al. On remote temperature sensing using commercial UHF RFID tags[J]. IEEE Internet of Things Journal, 2019, 6(6): 10715-10727.

[4] ZHANG J, MAO S, PERIASWAMY S C G, et al. Standards for passive UHF RFID[J]. ACM GetMobile, 2019, 23(3): 10-15.

[5] TAN W C, SIDHU M S. Review of RFID and IoT integration in supply chain management[J]. Operations Research Perspectives, 2022, 9: 100229.

[6] WANG X J, LIU Z, LIU A X, et al. A near-optimal protocol for continuous tag recognition in mobile RFID systems[J]. IEEE/ACM Transactions on Networking, 2023, 32(2): 1303-1318.

[7] MONDAL S, CHU Y H, CUDDIHY M, et al. Hybrid RFID based batteryless seat sensor with discontinuous RF transmission[J]. IEEE Transactions on Vehicular Technology, 2022, 71(3): 2305-2318.

[8] XU J R, LI Z, ZHANG K, et al. The principle, methods and recent progress in RFID positioning techniques: a review[J]. IEEE Journal of Radio Frequency Identification, 2023, 7: 50-63.

[9] VALENTINI R, DI MARCO P, ALESII R, et al. Cross-layer analysis of multi-static RFID systems exploiting capture diversity[J]. IEEE Transactions on Communications, 2021, 69(10): 6620-6632.

[10] MOTRONI A, BUFFI A, NEPA P. A survey on indoor vehicle localization through RFID technology[J]. IEEE Access, 2021, 9: 17921-17942.

[11] GUO W, HUANG C, QIN X, et al. Dynamic clustering and power control for two-tier wireless federated learning[J]. IEEE Transactions on Wireless Communications, 2024, 23(2): 1356-1371.

[12] LIN S, MIAO F, ZHANG J B, et al. ATPC: adaptive transmission power control for wireless sensor networks[J]. ACM Transactions on Sensor Networks, 2016, 12(1): 1-31.

[13] BONDADE R, MA D S. Hardware-software codesign of an embedded multiple-supply power management unit for multicore SoCs using an adaptive global/local power allocation and processing scheme[J]. ACM Transactions on Design Automation of Electronic Systems, 2011, 16 (3): 1-27.

[14] ALOTAIBI M, MURAD M, TASADDUQ I A, et al. Anti-collision algorithm for identification in precision agriculture applications[J]. IEEE Access, 2023, 11: 130197-130205.

[15] AMOAH B, WANG X Y, ZHANG J, et al. RFIDNet: a protocol for effective multiple RFID readers collaboration[C]//Proceedings of IEEE ICC 2025. Piscataway: IEEE Press, 2025: 6162-6167.

[16] LUO W C, ZHENG J L. RFID reader antenna optimal deployment based on improved elephant herding algorithm[C]//Proceedings of 2021 IEEE International Conference on Consumer Electronics and Computer Engineering. Piscataway: IEEE Press, 2021: 348-352.

[17] CAPPELLI I. Autonomous sensing nodes for IoT applications[D]. Siena SI: Università degli Studi di Siena, 2023.

[18] CHEN S. Towards robust general-purpose backscatter with commodity radios[D]. Vancouver: Simon Fraser University, 2024.

[19] ALI R, LIU R, HE Y P, et al. Systematic review of dynamic multi-object identification and localization: techniques and technologies[J].

IEEE Access, 2021, 9: 122924-122950.
[20] GU B W, LI D, DING H Y, et al. Breaking the interference and fading gridlock in backscatter communications: state-of-the-art, design challenges, and future directions[J]. IEEE Communications Surveys & Tutorials, 2025, 27(2): 870-911.
[21] SATHISHKUMAR P, RAJAN C, GEETHA K. A constructive steiner graph matching for radio frequency identification device tag detection in wireless and Internet of things environment[J]. Wiley International Journal of Communication Systems, 2024, 37(11): 5788.
[22] SHARMA S, SHAKOOR A. Performance evaluation of slotted ALOHA anti-collision protocol for mobile RFID tags identification using NHPP[J]. International Journal of Advanced Trends in Computer Science and Engineering, 2021, 10(3): 1676-1682.
[23] DE BARROS F I E, SILVA I, COSTA D G, et al. A reliability and performance GSPN-based model for anti-collision RFID algorithms under noisy channels in industrial Internet of things[J]. Elsevier Computers in Industry Journal, 2021, 125: 103381.
[24] QIU X X, CHAWLA K. On the performance of adaptive modulation in cellular systems[J]. IEEE Transactions on Communications, 1999, 47(6): 884-895.
[25] YUKSEL M E. A rreview of ALOHA-based anti-collision protocols in RFID systems[J]. Academic Studies in Engineering, 2023: 183.
[26] HOTA L, NAYAK B P, KUMAR A, et al. An analysis on contemporary MAC layer protocols in vehicular networks: state-of-the-art and future directions[J]. MDPI Future Internet, 2021, 13(11): 287.
[27] KUMAR S, VERMA P K. A comparative study of collision avoidance medium access control protocols in Internet-of-things[J]. Inderscience International Journal of Cloud Computing, 2024, 13(2): 139-164.
[28] WANG L, LUO Z Q, GUO R M, et al. A review of tags anti-collision identification methods used in RFID technology[J]. MDPI Electronics, 2023, 12(17): 3644.
[29] LIN M C, YANG Y Q, CHANG C Y, et al. An uplink random access scheme based on ALOHA system assisted by gain division multiple access[J]. IEEE Access, 2023, 11: 28887-28895.
[30] RIAHI S, RIAHI A. Performance evaluation of random access methods for wireless systems[J]. Journal of Theoretical and Applied Information Technology, 2021, 99(7): 1594-1607.
[31] SHIU D. Efficient computation of tight approximations to Chernoff bounds[J]. Springer Computational Statistics, 2023, 38(1): 133-147.
[32] CHUNG K M, LAM H, LIU Z M, et al. Chernoff-Hoeffding bounds for Markov chains: generalized and simplified[J]. arXiv Preprint, arXiv: 1201.0559. 2012.
[33] AL-SAADI M, AL-GREER M, SHORT M. Reinforcement learning-based intelligent control strategies for optimal power management in advanced power distribution systems: a survey[J]. MDPI Energies, 2023, 16(4): 1608.
[34] HUANG Q H, HUANG R K, HAO W T, et al. Adaptive power system emergency control using deep reinforcement learning[J]. IEEE Transactions on Smart Grid, 2020, 11(2): 1171-1182.
[35] TABAK A, İLHAN İ. An effective method based on simulated annealing for automatic generation control of power systems[J]. Elsevier Applied Soft Computing, 2022, 126: 109277.
[36] LEE K Y, EL-SHARKAWI M A. Modern heuristic optimization techniques: theory and applications to power systems[M]. Hoboken: John Wiley & Sons, 2008.
[37] TATARENKO T, KAMGARPOUR M. On the rate of convergence of payoff-based algorithms to Nash equilibrium in strongly monotone games[J]. arXiv Preprint, arXiv: 2202.11147. 2022.
[38] GADJOV D, PAVEL L. On the exact convergence to Nash equilibrium in hypomonotone regimes under full and partial-decision information [J]. IEEE Transactions on Automatic Control, 2022, 68(8): 4539-4553.
[39] SASTRY S. Lyapunov stability theory[M]// New York, NY: Springer, 1999.
[40] KONG Y J, LIU L, CHEN H H, et al. Overcoming catastrophic forgetting in continual learning by exploring eigenvalues of hessian matrix[J]. IEEE Transactions on Neural Networks and Learning Systems, 2023, 35(11): 16196-16210.
[41] LIU J Q, YU G H. Fuzzy Kakutani-Fan-Glicksberg fixed point theorem and existence of Nash equilibria for fuzzy games[J]. Elsevier Fuzzy Sets and Systems, 2022, 447: 100-112.
[42] BELLA P, SCHÄFFNER M. Lipschitz bounds for integral functionals with (p, q)-growth conditions[J]. Advances in Calculus of Variations, 2022, 17(2): 373-390.
[43] KUMAR K, SHARMA G, CHATURVEDI A K. Application of Friis transmission equation for power delay profile in Gaussian scattering [J]. Authorea Preprints, 2025: 1-6.

APPENDIX

A) Theoritical Analysis of Stability and Convergence: To establish the stability and convergence of our proposed algorithm, we expand Eq. (9) and prove that, despite the decentralized nature of decision-making, the algorithm converges to a stable Nash equilibrium[37-38]. This is achieved by leveraging Lyapunov stability analysis[39] and contraction mapping techniques, ensuring that the distributed power control mechanism remains robust, efficient, and scalable in dense RFID environments.

A.1) Utility Function: To ease of elaboration and analysis, we re-write the utility function as

$$u_i(P_i, P_{-i}) = R_i(P_i, P_{-i}) - C_i(P_i), \tag{A.1}$$

where $R_i(P_i, P_{-i}) = \sum_{T_j \in T_i} \sigma[S_{i,j}(t) \geqslant S_{\text{thresh}}] - \lambda_1 I_{\text{sum}}(R_i, t)$ is the revenue function, and $C_i(P_i) = \lambda_2 P_i^2$ is the cost function.

Existence of Nash Equilibrium: To prove the existence of a Nash equilibrium from Eq. (11), we rely on the following sufficient conditions.

- The strategy space $[P_{\min}, P_{\max}]$ is a closed and bounded interval, being compact and convex.
- The utility function $u_i(P_i, P_{-i})$ is concave in P_i because

$$\frac{\partial^2 u_i}{\partial P_i^2} = \frac{\partial^2 R_i}{\partial P_i^2} - 2\lambda_2. \tag{A.2}$$

Assuming $\frac{\partial^2 R_i}{\partial P_i^2} \leqslant 0$ (revenue decreases with increasing power), and since $\lambda_2 > 0$, it follows that the Hessian matrix[40] $\boldsymbol{H}_i$ is negative definite.

$$\boldsymbol{H}_i = \frac{\partial^2 u_i}{\partial P_i^2} < 0, \quad \text{ensuring concavity.} \tag{A.3}$$

- The continuity of $u_i(P_i, P_{-i})$ follows from the assumed continuity of $R_i(P_i, P_{-i})$ and $C_i(P_i)$.

Hence, by the Debreu-Glicksberg-Fan theorem[41], a Nash equilibrium $\boldsymbol{P}^* = (P_1^*, P_2^*, \cdots, P_N^*)$ exists. This implies that

no reader can improve its utility by unilaterally changing its power level.

Convergence of Adaptive Algorithm: The best response for a reader R_i is defined by

$$P_i^{(k+1)} = \arg\max_{P_i} \left\{ u_i(P_i, P_{-i}^{(k)}) \right\}. \tag{A.4}$$

The adaptive power control algorithm updates the power levels iteratively using the gradient ascent method

$$P_i^{(k+1)} = P_i^{(k)} + \gamma \frac{\partial u_i}{\partial P_i}\bigg|_{P_i^{(k)}, P_{-i}^{(k)}}, \tag{A.5}$$

where $\gamma > 0$ is the learning rate controlling the update step size and it is chosen such that the Lipschitz condition[42] $L = \gamma \max_i \left| \frac{\partial^2 u_i}{\partial P_i^2} \right| < 1$ is satisfied.

Monotonicity of Utility Improvement: At each iteration k, the utility $u_i(P_i^{(k+1)}, P_{-i}^{(k)})$ satisfies

$$u_i(P_i^{(k+1)}, P_{-i}^{(k)}) \geqslant u_i(P_i^{(k)}, P_{-i}^{(k)}). \tag{A.6}$$

- Applying Taylor expansion, we have

$$u_i(P_i^{(k+1)}, P_{-i}^{(k)}) \approx u_i(P_i^{(k)}, P_{-i}^{(k)}) + \gamma \left(\frac{\partial u_i}{\partial P_i}\bigg|_{P_i^{(k)}, P_{-i}^{(k)}} \right). \tag{A.7}$$

- By the gradient ascent update rule, $\frac{\partial u_i}{\partial P_i}\big|_{P_i^{(k)}, P_{-i}^{(k)}} \geqslant 0$, ensuring

$$u_i(P_i^{(k+1)}, P_{-i}^{(k)}) - u_i(P_i^{(k)}, P_{-i}^{(k)}) \geqslant 0. \tag{A.8}$$

Thus, the utility of each reader is non-decreasing at every iteration, ensuring monotonic improvement.

Contraction Mapping and Convergence: Let $\boldsymbol{P}^{(k)} = (P_1^{(k)}, P_2^{(k)}, \cdots, P_N^{(k)})$ represent the power vector at iteration k. The algorithm forms a contraction mapping

$$\|\boldsymbol{P}^{(k+1)} - \boldsymbol{P}^*\| \leqslant c \|\boldsymbol{P}^{(k)} - \boldsymbol{P}^*\|, \quad c \in [0,1), \tag{A.9}$$

where $\boldsymbol{P}^*$ is the Nash equilibrium and the following hold.

(i) The contraction constant c depends on the curvature of the utility function $u_i(P_i, P_{-i})$.

(ii) The concavity of $u_i(P_i, P_{-i})$ ensures diminishing gradients as $P_i \to P_i^*$.

(iii) The update rule is a contraction if the Jacobian matrix $\boldsymbol{J}_{ij} = \frac{\partial P_i^{(k+1)}}{\partial P_j^{(t)}}$ of the mapping satisfies $\|\boldsymbol{J}\| < 1$.

Thus, gradient ascent update satisfies the contraction mapping property, leading to convergence

$$\lim_{k \to \infty} \boldsymbol{P}^{(k)} = \boldsymbol{P}^*. \tag{A.10}$$

Fixed Point and Convergence: After convergence, $P_i^{(k+1)} = P_i^{(k)} = P_i^*$, satisfying the Nash equilibrium condition

$$\frac{\partial u_i}{\partial P_i}\bigg|_{P_i^*, P_{-i}^*} = 0, \quad \forall i \in \mathcal{N}. \tag{A.11}$$

This condition ensures that no reader can unilaterally improve its utility by adjusting its power level, confirming that $\boldsymbol{P}^*$ is stable. To verify the uniqueness of $\boldsymbol{P}^*$, we employ the Lyapunov stability theory[39], which provides a framework for analyzing the behavior of dynamic systems over time. It states that a system is considered stable if, starting from an initial state, it returns to equilibrium or remains bounded.

Lyapunov Function Definition: A Lyapunov function $V(\boldsymbol{P}(t))$ for the distributed power control system is defined as

$$V(\boldsymbol{P}(t)) = \frac{1}{2} \sum_{i=1}^{N} \left(u_i(P_i(t), P_{-i}(t)) - u_i(P_i^*, P_{-i}^*) \right)^2, \tag{A.12}$$

where $u_i(P_i, P_{-i})$ represents the utility function of reader R_i and $P^* = (P_1^*, P_2^*, \cdots, P_N^*)$ is the Nash equilibrium power configuration. The Lyapunov function $V(\boldsymbol{P}(t))$ measures the deviation of the system's current state from the Nash equilibrium. For stability, $V(\boldsymbol{P}(t))$ must satisfy

$$V(\boldsymbol{P}(t)) > 0 \quad \forall \boldsymbol{P}(t) \neq \boldsymbol{P}^* \text{ and } V(\boldsymbol{P}^*) = 0. \tag{A.13}$$

Lyapunov Function Derivative: The time derivative $\dot{V}(\boldsymbol{P}(t))$ is given by

$$\dot{V}(\boldsymbol{P}(t)) = \sum_{i=1}^{N} (P_i(t) - P_i^*) \frac{\partial u_i(P_i(t), P_{-i}(t))}{\partial P_i}. \tag{A.14}$$

If $\frac{\partial u_i}{\partial P_i} < 0$ for all non-equilibrium states $\boldsymbol{P}(t) \neq \boldsymbol{P}^*$, then

$$\dot{V}(\boldsymbol{P}(t)) < 0. \tag{A.15}$$

This indicates that the Lyapunov function decreases over time, proving that $\boldsymbol{P}(t) \to \boldsymbol{P}^*$ as $t \to \infty$, which is the stable equilibrium point. Since the Lyapunov function $V(\boldsymbol{P}(t))$ satisfy

$$\dot{V}(\boldsymbol{P}(t)) \leqslant -k \|\boldsymbol{P}(t) - \boldsymbol{P}^*\|^2, \quad \text{for some } k > 0, \tag{A.16}$$

we conclude that the Nash equilibrium $\boldsymbol{P}^*$ is unique, leading to global stability.

A.2) Long-Term Behavior in Dynamic Environments: In practical RFID deployments, the system operates in dynamic conditions where tag density and interference levels may fluctuate over time. The proposed algorithm adapts to such variations by continuously recalibrating power levels based on real-time feedback. The long-term behavior is characterized by the following properties.

(i) System Stability: At Nash equilibrium, each reader operates at its optimal power level, ensuring the system reaches a stable configuration. Stability is vital in dense RFID environments to avoid oscillatory or unpredictable behavior caused by uncontrolled power adjustments.

(ii) Robustness to Environmental Changes: The algorithm remains robust to changes in tag density and interference levels by ensuring that each reader's power level is updated in response to environmental feedback. Let $\mathscr{E}(t)$ denote the environment state at time t, influencing the utility u_i and the update rule expressed as in (A.5). As $\mathscr{E}(t)$ changes, the system converges to a new Nash equilibrium, ensuring stable performance over time.

(iii) Energy Efficiency and Collision Mitigation: The long-term energy efficiency is guaranteed by minimizing the power cost $C_i(P_i)$ without sacrificing throughput. The collision probability P_{col} is reduced as readers stabilize at power levels that minimize interference. Experimentally, the system achieves a high throughput ($> 90\%$) even under dynamic conditions and energy savings ($> 30\%$) compared to static power allocation strategies.

(iv) Optimal Resource Utilization: Convergence ensures that readers minimize interference while maximizing throughput and power consumption is optimized, achieving energy efficiency without sacrificing tag detection accuracy. For example, readers avoid overusing power, which could degrade the overall system performance due to excessive interference.

(v) Avoidance of Suboptimal Strategies: Without convergence some readers might underutilize their power, leading to missed tag reads and others might overuse power, causing excessive interference. Convergence ensures that all readers reach a mutually optimal state, avoiding these inefficiencies.

A.3) Theoretical Guarantees of Stability:

To summarize, the proposed algorithm guarantees global stability and robust long-term behavior due to: (i) The concavity of the utility function $u_i(P_i, P_{-i})$, ensuring a unique Nash equilibrium. (ii) The monotonic improvement of utility at each iteration. (iii) The contraction mapping property guarantees convergence to a stable fixed point. (iv) Adaptability to dynamic environments, enabling the system to recalibrate and maintain efficiency. These theoretical guarantees are supported by both analytical derivations and experimental validations, as presented in section VI.

B) Scalability Analysis in Terms of Coverage

B.1) Coverage Area per Reader: The coverage area A_{coverage} of a single reader within the total area of deployment, $A_{\text{deployment}}$, depends on its coverage radius r_{coverage}, which is determined by the received signal strength at a tag. The minimum detectable signal strength $P_{\min}$ at a tag is related to the reader's transmit power T_i by the Friis equation[43]

$$P_{\min} = T_i G_t G_r \left(\frac{\lambda}{4\pi r_{\text{coverage}}}\right)^2, \tag{B.1}$$

where G_t is the reader antenna gain, G_r is the tag antenna gain, λ is the wavelength of the transmitted signal, and r_{coverage} is the reader's coverage radius. Rearrange it to find r_{coverage}

$$r_{\text{coverage}} = \left(\frac{T_i}{P_{\min}} G_t G_r \left(\frac{\lambda}{4\pi}\right)^2\right)^{\frac{1}{2}}. \tag{B.2}$$

For simplicity, let $\mathrm{C}_1 = G_t G_r \left(\frac{\lambda}{4\pi}\right)^2$. To account for path loss in realistic environments, we introduce the path loss exponent η, leading to

$$r_{\text{coverage}} = \left(\mathrm{C}_1 \frac{T_i}{P_{\min}}\right)^{\frac{1}{\eta}}. \tag{B.3}$$

The coverage area of a single reader is given by

$$A_{\text{coverage}} = \pi \left(\mathrm{C}_1 \frac{T_i}{P_{\min}}\right)^{\frac{2}{\eta}} = C_2 \left(\frac{T_i}{P_{\min}}\right)^{\frac{2}{\eta}}, \tag{B.4}$$

where $\mathrm{C}_2 = \pi C_1^{\frac{2}{\eta}}$.

B.2) Total Coverage with N Readers: For a network with N readers, the total theoretical coverage is

$$A_{\text{total}} = N A_{\text{coverage}} = N \mathrm{C}_2 \left(\frac{T_i}{P_{\min}}\right)^{\frac{2}{\eta}}. \tag{B.5}$$

However, in dense deployments, overlaps between interrogation zones reduce the effective coverage. Assuming overlaps scale as $\mathscr{O}(N^2)$, the effective coverage becomes

$$A_{\text{effective}} = A_{\text{total}} - \text{Overlaps}. \tag{B.6}$$

Using Overlaps $\sim \mathscr{O}(N^2)$, the effective coverage simplifies to

$$A_{\text{effective}} \sim \mathscr{O}\left(N T_i^{\frac{2}{\eta}} - N^2\right). \tag{B.7}$$

B.3) Scalability Across Deployment Densities:

1) Low-Density Deployments ($N \ll A_{\text{deployment}}$): In low-density deployments, the overlap between interrogation zones is negligible, so the effective coverage scales linearly with the number of readers

$$A_{\text{effective}} \sim N A_{\text{coverage}} \sim \mathscr{O}(N). \tag{B.8}$$

2) High-Density Deployments ($N \gg A_{\text{deployment}}$): In high-density deployments, overlaps dominate, reducing the effective coverage. To mitigate interference, the system dynamically reduces the transmit power of each reader. If the power scales as

$$P_i \sim \mathscr{O}\left(\frac{1}{N}\right), \tag{B.9}$$

then the coverage area of a single reader becomes

$$A_{\text{coverage}} \sim \mathscr{O}\left(\left(\frac{1}{N}\right)^{\frac{2}{\eta}}\right). \tag{B.10}$$

The total effective coverage is then given by

$$A_{\text{effective}} = NA_{\text{coverage}} = \mathcal{O}\left(N^{1-\frac{2}{\eta}}\right). \tag{B.11}$$

For the case of free space, we have $\eta = 2$. Thus $A_{\text{effective}} = \mathcal{O}(1)$. The algorithm allows for efficient scaling without interference in low-density environments, supporting linear scalability. In high-density environments, the dynamic adjustment of transmit power ($P_i \sim \mathcal{O}(1/N)$) ensures stable performance despite saturation ineffective coverage. This validates the algorithm's ability to manage dense deployments effectively.

About the Authors

Bernard Amoah (Graduate Student Member, IEEE) is a Ph.D. student in electrical engineering at Auburn University, Auburn, USA, specializing in wireless communication, and RFID technology. He holds a B.Sc. in computer engineering from Kwame Nkrumah University of Science and Technology (KNUST), Ghana. With over 12 years of industry experience, he has led major telecommunications, IT, and fintech projects. He has held leadership roles such as Senior Software Project Manager, and Chief Technology (Technical) Officer in the IT and Telecommunication space. His expertise spans RFID systems, IoT, fiber optics, IT infrastructure, and AI-driven network optimization. Currently, he is a Graduate Research Assistant at Auburn University RFID Lab, focusing on machine learning for wireless networks, RFID-based communication, and IoT-driven data acquisition.

Xiangyu Wang (Member, IEEE) received the Ph.D. in electrical and computer engineering from Auburn University, Auburn, USA, in 2022. Currently, he is a Postdoctoral Researcher at Auburn University RFID Lab. Before joining the RFID Lab, he worked as an Embedded Software Engineer for SML RFID. His research interests include wireless sensing, smart health, the Internet of things (IoT), and IoT security. In addition, he is also interested in interdisciplinary topics that involve deep learning, indoor localization, and radio frequency identification (RFID).

Jian Zhang (Member, IEEE) received the B.Sc. and M.Sc. degrees in applied physics from Sichuan University, Chengdu, China, in 2001 and 2008, respectively, and the Ph.D. degree in electrical and computer engineering from Auburn University, Auburn, USA, in 2016. Currently, he is an Assistant Professor in the Department of Information Technology at Kennesaw State University, Kennesaw, USA His main research interests include automated and intelligent robotic systems involving machine learning, autonomous robotics, indoor wireless localization, and RFID applications. He is a co-recipient of the Runner-up of the Best Paper Award of IEEE CCNC 2022 and IEEE GLOBECOM 2023 Best Paper Award (BPA) for the IoT and Sensor Networks.

Shiwen Mao [corresponding author] (Fellow, IEEE) received the Ph.D. degree in electrical engineering from Polytechnic University, Brooklyn, USA, in 2004. In 2006, he joined Auburn University, Auburn, as an Assistant Professor in the Department of Electrical and Computer Engineering. He held the McWane Endowed Professorship from 2012 to 2015 and the Samuel Ginn Endowed Professorship from 2015 to 2020. Currently, he is a Professor and Earle C. Williams Eminent Scholar, and Director of the Wireless Engineering Research and Education Center at Auburn University. His research interests include wireless networks, multimedia communications, and smart grid. He is the editor-in-chief of IEEE Transactions on Cognitive Communications and Networking, a member-at-large on the Board of Governors of IEEE Communications Society, and Vice President of Technical Activities of IEEE Council on Radio Frequency Identification (CRFID). He received the IEEE ComSoc MMTC Outstanding Researcher Award in 2023, the SEC 2023 Faculty Achievement Award for Auburn, the IEEE ComSoc TC-CSR Distinguished Technical Achievement Award in 2019, the Auburn University Creative Research & Scholarship Award in 2018, the NSF CAREER Award in 2010, and several service awards from IEEE ComSoc. He is also a co-recipient of the 2022 Best Journal Paper Award of IEEE ComSoc eHealth Technical Committee, the 2021 Best Paper Award of Elsevier/KeAi Digital Communications and Networks Journal, the 2021 IEEE Internet of Things Journal Best Paper Award, the 2021 IEEE Communications Society Outstanding Paper Award, the IEEE Vehicular Technology Society 2020 Jack Neubauer Memorial Award, the 2018 Best Journal Paper Award and the 2017 Best Conference Paper Award from IEEE ComSoc MMTC, and the 2004 IEEE Communications Society Leonard G. Abraham Prize in the field of communications systems. He is a co-recipient of the Best Paper/Demo Awards of 12 conferences.

Senthilkumar C.G. Periaswamy received the Ph.D. degree in computer science from University of Arkansas Fayetteville, Fayetteville, USA, in 2010. He is currently the Director of Technology for the RFID lab at Auburn University, a unique collaboration platform that involves end users, suppliers, technology providers, standards organizations, industry groups, and academic institutions on a global scale. He has researched, advised, and executed projects that enable efficient adoption of RFID and sensor fusion in retailing, aerospace, manufacturing, and transportation. His research interests include the common goal of making the adaptation of RFID and related sensor technologies more secure, efficient, reliable and useful.

Justin Patton is the Director of the Auburn University RFID Lab, Auburn, USA, a research institute focusing on the business case and technical implementation of emerging technologies in retail, supply chain, aerospace, and manufacturing. The RFID Lab is a unique private/academic partnership between users, technology vendors, standards organizations, and faculty. He has participated in business case research for advanced technology with Walmart, Target, Amazon, FedEx, Dillard's, Macy's, Delta Air Lines, and Boeing among others, and is currently researching upstream supply chain benefits of RFID in both retail and manufacturing. He is one of the primary developers of the ARC program, the first and most widely utilized international performance validation system for RFID, and is currently working to help standardize the process of testing and certifying RFID performance in all aspects of the supply chain.